Universiteit Utrecht

Master Thesis

CP violation in Higgs production in association with two jets in vector boson fusion channel and gluon gluon fusion channel

Yasaman Fereydooni

Supervisor: Dr. Peter Kluit.

Utrecht University.

Faculty of Science/Department of Physics and Astronomy.

CP violation in Higgs production in association with two jets via Vector Boson Fusion channel and gluon gluon Fusion channel

---

***Abstract**: Determining the CP-state of the recently discovered Higgs boson at the LHC is a matter of great importance.*
In this analysis, the Monte Carlo simulated signal samples have been used to study the kinematics of the two tagged jets in Higgs production via the Vector Boson Fusion (VBF) and the gluon gluon Fusion (ggF) channels to determine the CP properties of the Higgs boson. For comparison and development of observables to distinguish a CP-even from a CP-odd Higgs boson in $H \rightarrow WW \rightarrow l\nu l\nu$, first the signal region needs to be improved, thus, a set of optimal selection criteria is developed for both channels. Then, the "classical variable" $\Delta\Phi_{jj}$ i.e. the azimuthal angle between the jets, which is a CP-sensitive variable in both channels, is used to study and distinguish the behavior of Higgs CP-odd and Higgs CP-even.
The shape of the $\Delta\Phi_{jj}$ distribution can be predicted for both CP- states based on the matrix element in both channels. Therefore by fitting the $\Delta\Phi_{jj}$ distribution with a function which is extracted from the matrix element, for different slices of $\Delta\eta_{jj}$, the CP-even Higgs boson is distinguished from a CP-odd Higgs boson.

CONTENT

PREFACE

"This is a great breakthrough, one that could be profoundly significant to our understanding of the universe and the fundamental laws that govern it."

British Prime Minister David Cameron.

The Higgs boson discovery is certainly, the biggest achievement of this century in particle physics. The better understanding of the Higgs boson properties would lead to have a better picture of our universe.

The Higgs boson had been a last missing piece of the Standard Model for more than 40 years and after its magical discovery, it has become a superstar in most of the experimental scenarios in physics.

The aim of this manuscript is to study and measure the CP-state of the Higgs boson based on the prediction of some theories beyond the Standard Model.

Chapter 1 reviews the LHC experiment with a focus on the ATLAS detector.

Chapter 2 gives and introduction to the Standard Model of the elementary particles with a short review on the electroweak unification and the Higgs Mechanism followed by the properties of the Standard Model Higgs boson. Then the extension of the Higgs boson beyond the standard model with a focus on the ggF and the VBF production channels is discussed

Chapter 3 starts with an introduction to event generation followed by the summery of the analysis setup and signal sample simulations. Then the analysis and the results are given and interpreted.

Chapter 4 chapter summarizes the results and concludes the thesis.

1 INTRODUCTION TO THE LHC AND THE ATLAS DETECTOR

The large hadron collider (LHC), is the biggest and the most powerful experimental lab in the world. It is located at CERN, at the border between France and Switzerland. This big collider has been built to test the predictions of the different theories and hypothesizes in particle physics, and expand the physics borders. One of the main motivation to build the biggest international collider, was to search for evidence of the predicted Higgs boson. After the discovery of the Higgs boson in 2012, the LHC has continued the performance, aim to explore more about the new physics and new particles.

The LHC is built in a tunnel which is located approximately 100 m below the ground with a circumference of 27 km. This collider contains two proton beams ($\sim 3.10^6$ protons per cm^3) that travel oppositely through two separate beam pipes which have intersections at four points. At these intersection points, detectors for four main experimental projects are located: A Toroidal LHC ApparatuS (ATLAS), Compact Muon Solenoid (CMS), Large Hadron Collider beauty (LHCb) and A Large Ion Collider Experiment (ALICE). The LHC was designed to operate at the center of mass energy of $\sqrt{s} = 7\ TeV$ for the colliding protons in the run1. By 2015, the LHC was upgrated and reached the center of mass energy of $\sqrt{s} = 14\ TeV$ at the luminosity of $10^{34} cm^{-2} s^{-1}$. [1-3].

As this thesis has been done in the ATLAS group, in the next section, a short review of the ATLAS detector is given.

1.1 The ATLAS detector

ATLAS detector is the biggest particle detector in the world which has a 44 meters of length, 25 meters of height and 7000 tons of weight. This detector is forward-backward symmetric with almost full solid angle coverage around the interaction point. This general purpose detector is designed to operate for different physical experiments and explore the full spectrum of the proton proton collision. This detector has a cylindrical shape around the interaction point and is composed of four sub-detectors: the Inner Detector (ID) or inner tracker, the Electromagnetic Calorimeter (ECal), the Hadronic Calorimeter (HCal) and the Muon Spectrometer (MS). The schematic cross section of the ATLAS detector with the position of its sub-detectors is shown in figure 1. [4-6].

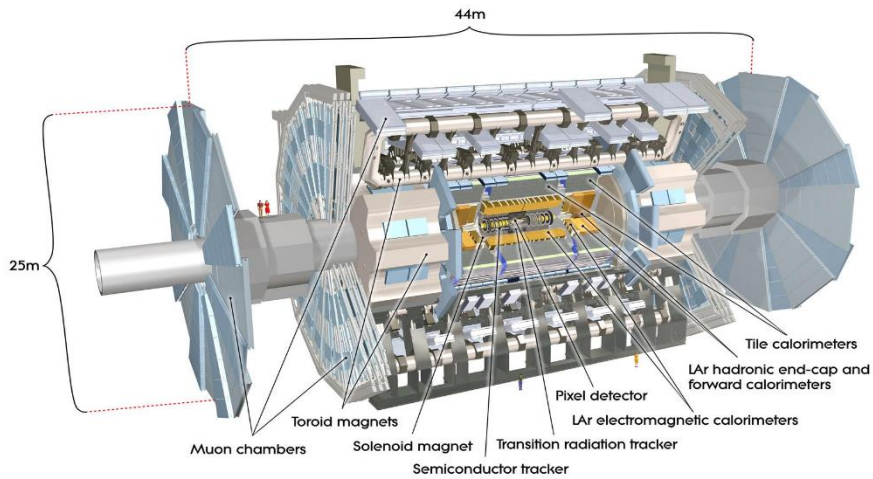

Figure 1.The schematic view of the ATLAS detector with all the different parts.

1.1.1 The ATLAS coordinate system:

To describe the location of the particles and the interaction points, a coordinate system needs to be defined. The ATLAS detector has a right handed coordinate system with the z-axis along the LHC beam pipe where its origin is in the nominal interaction point of ATLAS. The x-y plane which is called the transverse plane, is perpendicular to the z-axis. The azimuthal angle which is the angle around the beam axis, is denoted by $\Phi \in (-\pi, \pi)$ and the polar angle which is defined as the angle between momentum and the z-axis is represented by $\theta \in (0, \pi)$. Another important parameter which depends on θ, is called pseudo rapidity and is shown by η. This parameter is more often used to define the position and the direction of a particle in the detector and is defined as $\eta = -ln(tan(\theta/2))$. [1,7].

1.1.2 Magnet

ATLAS detector has two large superconducting magnets. A superconducting solenoid with the length of 5.8 m and the axial magnetic field of 2 T in the center of the inner detector and a toroidal magnet inside the Muon Spectrometer. The toroidal magnet provides a field of 0.5 to 1 T on average. One of the functionality of the magnetic fields is to bend the trajectory of the charged particles to measure their momentum. [8].

1.1.3 Inner detector

The ATLAS inner detector is surrounded by the superconducting solenoid magnet system. As it is the closest part of the ATLAS detector to the beam axis, it is responsible to provide information about the charged particles track, impact parameter with resolution of 10 μm and the transverse momentum with resolution of $\frac{\sigma_{PT}}{P_T} = 0.05\%\ P_T \oplus 1\ \%$. Inner detector has the pseudo-rapidity acceptance of $|\eta| \leq 2.5$ for particles coming from the interaction region. The ATLAS inner detector consists of three subsystems which are the pixel detector, the silicon strip detector (SCT) and the transition radiation tracker (TRT). The profile of the inner tracker is shown in figure 2. The pixel detector and the silicon strip detector are based on silicon semiconductor modules while the transition radiation tracker is based on gaseous drift tubes [1,7,9].

-The pixel detector: This subsystem is responsible for precise measurement of the position of the particles. The system consists of three layers of barrels with radii of 5.9 cm, 9 cm and 12 cm and three endcaps. The detector has 1744 silicon pixel modules which are made from 250 μm thick n-type silicon and each module contains 16 readout chips. All the layers combined together, contain more than 80 million pixels. Since pixel detector is located close to the interaction point, it is exposed to high radiation, so all the modules are required to have high radiation hardness. As the charged particles first cross the pixel detector, this detector provides information on impact parameter, coordinates of the interaction point and identifying short lived particles.

-**The silicon strip detector:** This part, consists of 4088 silicon micro-strip modules instead of pixels. These modules are arranged in four concentric barrel layers and two end caps with 9 disks in each. The SCT covers the radial distance of 299 mm to 560 mm. The SCT is responsible for tracking in the plane perpendicular to the beam, and it provides a 3-D space-point measurements.

-T**he transition radiation tracker:** This subsystem is the outermost layer of the ID and is built in the form of straw tube. It contains 3.7×10^5 straw tubes with diameter of 4 mm. In this subdetector, the detecting elements are drift tubes (straw) that each is filled with a Xenon based gas mixture and is surrounded by a dielectric material in a way that the tube's wall acts as a cathode. When a charged particle travels in a tube, it ionizes the Xeons gas and produces transition radiation photons. The electron identification can be done by detecting the transition radiation of these produced photons. The number of photons that are produced by radiation are proportional to the relativistic factor of the particle, i.e. $\gamma=\frac{E}{m}$, so the type of the charged particle can be identified by the number of the produced photons.

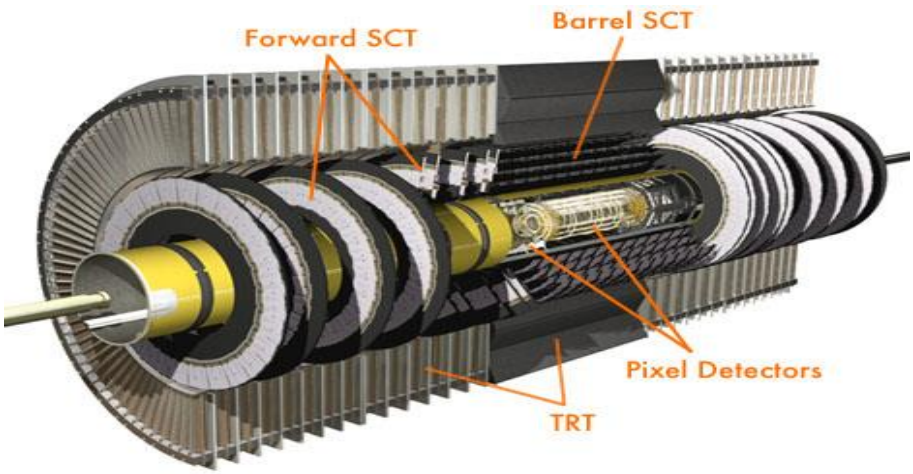

Figure 2. The view of the ATLAS detector with its subsystems.

1.1.4 The calorimeter system

The calorimeter system where is located outside the solenoid magnet, is divided into three subsystems: Electromagnetic CALorimeter (ECAL), Hadronic CALorimeter (HCAL) and Forward CALorimeter (FCAL). ECAL and HCAL both on average have coverage of $|\eta|<4.9$. The main task of this system is providing precise measurements on the energy of the particles, triggering and estimating the missing energy. Each subsystem is built from a dense absorbing material and an active medium. When particles travel across the calorimeter system, they interact with absorbing material and lose their energy and they produce electromagnetic or hadronic shower of particles. The produced shower can be detected and be measured in the active medium of the calorimeter for particle identification. In ECAL, Pb plates are used as absorbing materials and liquid argon as an active material. The ECAL covers a pseudo-rapidity interval of $|\eta|<3.2$ and it consists of a barrel and two end caps. When charged particles like electrons, travel through the absorbing material, they lose energy by Bremsstrahlung or pair production/annihilation. These mechanisms produce electromagnetic showers of particles that ionizes the active material which generate electric signal proportional to energy lost. This signal can be used for particle identification. The HCAL, is responsible for energy measurement of the particles that did not produce shower in ECAL. These particles which are hadrons, produce hadronic shower when they interact with the absorbing material of the HCAL. As the absorbing material of the HCAL is denser, it has a larger stopping power that stops the hadronic shower within the HCAL. Then the energy of the shower can be measured.

The outermost subsystem which is FCAL, provides measurements on both hadronic and electromagnetic showers in the most forward region. FCAL has a good hermetic coverage$3.1<|\eta|<4.9$ which helps to determine the missing transverse energy [6,7,10,11].

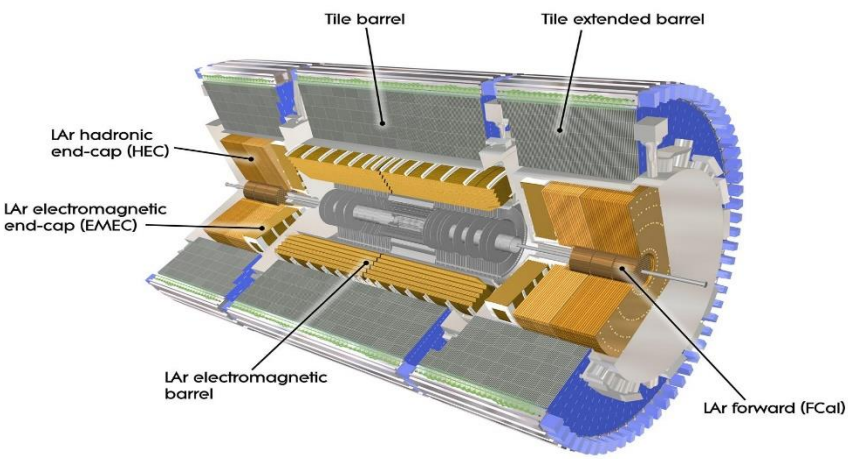

Figure 3. A cross section of the ATLAS calorimeter. The location of the hadronic calorimeter and electromagnetic calorimeter are shown in the picture.

1.1.5 The muon spectrometer

The muon spectrometer which is the largest part of the ATLAS detector, has the most distance from the interaction point. Muon spectrometer consists of three parts: three toroidal magnets, triggering system and measuring system to measure the track of outgoing muons precisely. The muon spectrometer starts from a radius of 4.25 m from outside of the calorimeter to the radius of 11 meter which is the radius of the full ATLAS detector. This subdetector is responsible to construct the muon track and measure their kinematics like momentum. The momentum measurement is done with the help of the magnetic fields which bend the trajectory of the muons [1,6,7,12].

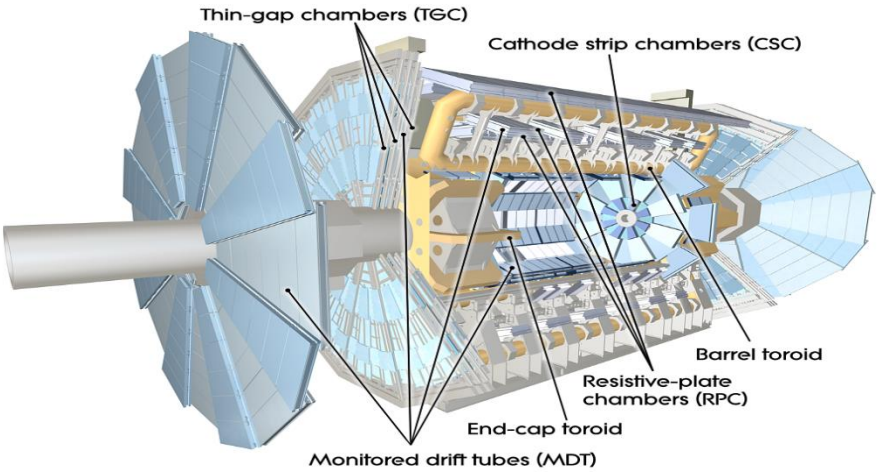

Figure 4. The schematic view of the Muon spectrometer

2 INTRODUCTION TO THEORY

The pursuit of the constituents of matter goes back to the late 5th century B.C. when Democritus, in the aim of understanding what the matter is made of, proposed his atomic theory which stated that all matters are composed of eternal, invisible and infinitely small substances. He called these small objects "atom" which means invisible. Search for the evidence of predicted atom started in 19th century by John Dalton and had become more advanced by discovery of electron in 1897 by Sir Joseph John Thompson. Now after 2500 years of proposing many different theories and experimenting, the Standard Model of the elementary particles is the only theory that provides a fundamental description of all the elementary particles.

In this chapter, a summary of the Standard Model including the electroweak theory and the Higgs mechanism is given. In the last section of this chapter, a short overview about some theories beyond the Standard Model with the focus on the Higgs boson is given.

2.1 The Standard Model of the elementary particles(SM)

The Standard Model (SM) is a robust theory that describes the elementary particles and their interaction and classifies them based on their properties. The SM is built based on the Quantum Field Theory and physical symmetries, it is a non-abelian theory with the gauge symmetry group $\mathrm{SU}(3)_C \times SU(2)_L \times U(1)_Y$ that describes particles, their interactions and fundamental forces except gravity. In order to fully describe the elementary particles, fundamental forces and interaction are described and formulated in the form of mathematical equations under the SM symmetries which are called Lagrangian. Elementary particles are classified by the SM based on their spin in two category, fermions with half integer spin and bosons with integer spin. For every fermion and boson, the existence of an associated anti-particle with the same mass and opposite quantum numbers is predicted by the SM.

-Bosons:

This category of particles which are also known as the force particles, have integer spin and they obey the Bose-Einstein statistics. Some of these particles that have spin-1, mediate the fundamental forces, for instance: massless photons and gluons, massive $W^{\pm}$ and Z^0 , which are all called gauge vector bosons. Higgs particle which is another example of bosons, has spin zero and is responsible for mass generation.

-Fermions:

Fermions or matter particles, have half integer spin and they obey the Fermi Dirac statistics. Fermions are divided in two categories: quarks and leptons and each category is also divided into three families.

Each family of quarks consist of an up-type quark with electric charge of 2/3 and a down- type quark with electric charge of 1/3. The masses of the quarks increase in each family. The first family of quarks contains the stable quarks that are recognized to be the constituents of the ordinary matter. The second and the third family have higher masses and they are unstable.

Each family of leptons contains a charged electron-like lepton and a neutral neutrino. The first generation consists of an electron with electric charge -1 and an electron-neutrino, the second generation consists of a muon with electric charge -1 and a muon-neutrino and the third one consists of a tau with electric charge -1 and a tau-neutrino. The masses of the electron- like leptons increase in each family.

-Fundamental forces and their mediators:

There are four fundamental forces in nature: electromagnetic, weak, strong and gravity. The SM only contains electromagnetic, weak and strong force and does not explain the gravity force. Each fundamental force in the SM is mediated by a vector boson (gauge boson).

The massless photon mediates the electromagnetic force. Photons don't have self-coupling. All the particles that have the quantum number electric charge, take part in the electromagnetic interaction. For instance, all the leptons and quarks can interact through the electromagnetic force.

Eight types of massless gluons mediate the strong force. They carry the quantum number called color. All quarks are subject to the strong force as they have the color charge.

The massive $W^{\pm}$ and Z^{0} bosons mediate the weak force. This force has relatively shorter range as its mediators are massive.

As it will be explained in section 2.2.2, the electromagnetic and weak force are unified in the SM as a context called electroweak force or electroweak interaction. All the fermions take part in the electroweak interaction.

Figure 5, shows the list of the Standard Model elementary particles.

More details about the SM are given in these books [13-14].

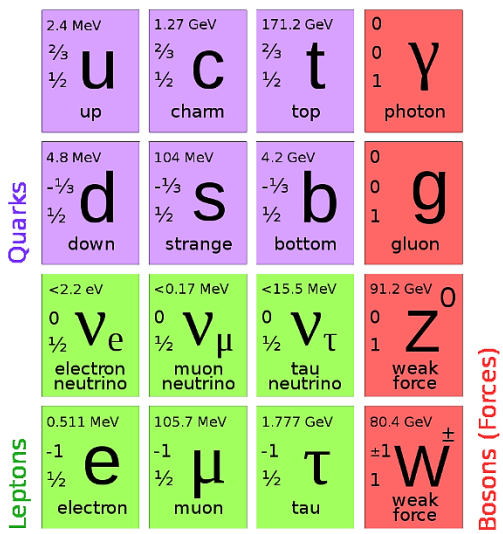

Figure 5: The SM elementary particles with their mass, electric charge and spin are shown

2.2 Mathematical foundation and theoretical descriptions of interactions in the SM

As the standard model is built based on the Quantum Field Theory and its symmetries, the equation of motion of all the particles and their interactions can be described by Lagrangian density.

The mathematical formalism of the SM is in a way that each fundamental interaction is described by a local gauge invariant symmetry group. For instance, the Quantum Electro Dynamics (QED) is described by the $\mathrm{U}(1)_{\mathrm{EM}}$ symmetry group and describes the interaction of the particles that carry electric charge, the Quantum Chromo Dynamics (QCD) is described by the $\mathrm{SU}(3)_C$ symmetry group and describes the interactions of the particles that carry the charge color and the unified theory of the electromagnetism and the weak force which is called electroweak interaction, is understood under the $\mathrm{SU}(2)_{\mathrm{L}} \times \mathrm{U}(1)_{\mathrm{Y}}$ electroweak symmetry group. QED, unified electroweak theory, QCD and the Higgs mechanism form the complete description of the SM and each of them are explained in the following sections.

2.2.1 Quantum Electro Dynamics (QED)

QED describes the dynamics and kinematics of the particles that undergo the electromagnetic interaction. In fact it describes and formulizes how photon and matter interact. As fermions obey the Dirac-Fermi statistics and they are the subject of QED, their dynamics are described by the Dirac Lagrangian which is the first building block of the full QED Lagrangian. We know from QFT that fermions are represented by Dirac spinor fields "ψ", so the Dirac Lagrangian for fermions can be written as;

$$L_{Dirac} = i\bar{\psi}\,\gamma^{\mu}\partial_{\mu}\psi - m\bar{\psi}\,\psi. \tag{2. 1}$$

Where γ^{μ} are the Dirac gamma matrices and $\bar{\psi}$ is the adjoint spinor field of the fermion which is defined as $\bar{\psi} = \psi^{+}\,\gamma^{0}$. The first term shows the kinetic energy and the second term represents the mass of the fermion. The Dirac Lagrangian is invariant under the $\mathrm{U}(1)_{\mathrm{EM}}$ symmetry group which is performed by a global phase transformation. The Dirac lagrangian does not contain a term that represents fermions interactions. In order to build up an interaction term for the fermions, a local phase transformation should be applied to Dirac spinors as;

$$\psi \rightarrow \psi' = e^{i\alpha(x)}\psi(x). \tag{2. 2}$$

but Dirac Lagrangian is not invariant under this transformation, to keep the Lagrangian unchanged, an additional gauge vector field should be introduced as $A_{\mu} = A_{\mu}(x)$ which can be added to the derivative term as;

$$D_{\mu} \equiv \partial_{\mu} - ieA_{\mu}(x). \tag{2. 3}$$

If we replace ∂_{μ} in the Lagrangian with D_{μ}, the obtained Lagrangian would have an interaction term between the fermion and the added gauge vector field as;

$$L_{Dirac} = i\bar{\psi}\,\gamma^{\mu}D_{\mu}\psi - m\bar{\psi}\,\psi = \bar{\psi}(i\,\gamma^{\mu}\partial_{\mu} - m)\psi - eA_{\mu}\bar{\psi}\,\gamma^{\mu}\psi. \tag{2. 4}$$

The vector field can be identified as the photon and e is the electric charge of the fermions. In order to be able to identify the vector field A_μ, with the physical field, i.e. photon and build the full QED Lagrangian, the kinetic term of the photon which is described by the field strength tensor $F_{\mu\nu}$, needs to be added to the Lagrangian as;

$$L_{kin} = -\frac{1}{4}F_{\mu\nu}(x)F^{\mu\nu}(x). \tag{2.5}$$

where $F_{\mu\nu} = \partial_\mu A_\mu - \partial_\nu A_\nu$ is the field strength tensor.

Consequently, the full Lagrangian which is invariant under the local gauge transformation and represents the electromagnetic interaction is given as;

$$L_{QED} = \underbrace{i\bar{\psi}\,\gamma^\mu\partial_\mu\psi}_{E_{kin}\,of\,fermions} - \underbrace{m\bar{\psi}\,\psi}_{mass\,of\,fermions} - \underbrace{eA_\mu\bar{\psi}\,\gamma^\mu\psi}_{interaction\,with\,photon} - \underbrace{\frac{1}{4}F_{\mu\nu}(x)F^{\mu\nu}(x)}_{E_{kin}\,of\,photon}. \tag{2.6}$$

More details about QED can be found in text books which are listed in references [1,6,7,13].

2.2.2 The electroweak unification

The dream of the grand unification of all the forces goes back to 1865 when Maxwell proposed the unification of electrostatic force and magnetic force into the electromagnetism theory and the research has retained by scientists aim to unify all the forces into one fundamental interaction. In 1979, Glashow, Salam and Weinberg were awarded the Nobel Prize for combination of the electromagnetism and the weak force. They showed that although these two forces may seem to be different at low energy scales, they can merge to a single force above a certain energy scale [15].

In the previous section, the formulation of the interaction of fermions with the photon field has been built by requiring the invariance of the Dirac Lagrangian under the $\mathrm{U(1)_{EM}}$ symmetry group. In this section, the same approach is pursued to build up the interaction terms for fermions with the massive $W^\pm$ and Z^0 bosons. Then in the attempt to unify electromagnetic force with weak force, the generator of the $\mathrm{U(1)_{EM}}$ group is represented by weak hyper charge instead of electric charge to make the symmetric group of $\mathrm{U(1)_Y}$, which all the fermions transform uniformly under this group. Then the unification of the electroweak theory is built based on the $\mathrm{SU(2)_L} \times \mathrm{U(1)_Y}$ symmetry group.

Weak hypercharge is a quantum number corresponding to electroweak interaction which relates the electric charge to the third component of the weak isospin. Their relation which is called the Gell-mann Nishijima formula [12] is represented by

$$Q = T_3 + \frac{Y}{2}. \tag{2.7}$$

All the fermions are divided to two categories based on their chirality, to left handed fermions and right handed fermions which have different weak isospin and weak hypercharge. Consequently, fermions are treated differently by weak interaction. The left handed fermions have weak isospin $\pm 1/2$ and transform as a doublet under $\mathrm{SU(2)_L}$ while right handed fermions transform as a singlet since they don't have weak isospin quantum number.

So we have: $\begin{pmatrix} \nu_i \\ l_i \end{pmatrix}_L$, $\begin{pmatrix} u_i \\ d_i \end{pmatrix}_L$, $(l_i)_R$, $(u_i)_R$, $(d_i)_R$, i=1,2,3.

The wave function of the left handed fermions is constructed by

$$\psi_L = \frac{1}{2}(1-\gamma^5)\psi. \tag{2.8}$$

And for the right handed fermions we have

$$\psi_R = \frac{1}{2}(1+\gamma^5)\psi. \tag{2.9}$$

In the previous section, the transformation of the Dirac spinor under the U(1) was checked. Now the transformation of the Dirac spinor under $\mathrm{SU}(2)_\mathrm{L}$ symmetry group should be considered. As the $\mathrm{SU}(2)_\mathrm{L}$ group has three generators that are represented by $T_a = \frac{1}{2}\sigma_a$,where σ_a are the Pauli matrices, it is a non-abelian group. By applying the local gauge transformation on the wave function, we have

$$\psi(x) \rightarrow \psi'(x) = e^{i\alpha^a(x)T_a}\psi(x), \text{a=1, 2, 3.} \tag{2.10}$$

To keep the Lagrangian invariant under the local gauge transformation, three gauge fields $W_\mu^a(x)$ need to be introduced that transform as;

$$W_\mu^a(x) \rightarrow W_\mu'^a(x) = W_\mu^a(x) + \frac{1}{g}\partial_\mu\alpha^a(x) + \epsilon_{abc}W_\mu^b\alpha^c(x), \text{a=1, 2, 3.} \tag{2.11}$$

where g is the coupling constant.

The covariant derivative also must to be re-defined as;

$$\partial_\mu \rightarrow D_\mu = \partial_\mu - igT_aW_\mu^a(x). \tag{2.12}$$

The W_μ^a with a=1,2,3 , are three gauge fields that they have physical interpretations, so the dynamic of them needs to be added as well by a kinetic term to Lagrangian as

$$L_{kin} = -\frac{1}{4}W_{\mu\nu}^a W_a^{\mu\nu}. \tag{2.13}$$

where $W_{\mu\nu}^a$ is the field strength tensor as we have has for A_μ in QED before and is defined as

$$W_{\mu\nu}^a = \partial_\mu W_\nu^a - \partial_\nu W_\mu^a. \tag{2.14}$$

So far four vector fields have been reconstructed, one for electromagnetic force A_μ, and three for the weak force W_μ = (W_1, W_2, W_3), so the unified electroweak theory should contain all these four fields.

The equation below shows the covariant derivative of the unified theory which is defined based on the implications from the symmetry group $\mathrm{SU}(2)_\mathrm{L} \times \mathrm{U}(1)_\mathrm{Y}$

$$D_\mu^{L,R} = \partial_\mu - igI_a^{L,R}W_\mu^a - i\frac{g'}{2}YB_\mu, \text{ with } I_a^L = \frac{1}{2}\sigma_a = T^a,\ I_a^R = 0. \tag{2.15}$$

where B_μ is a gauge field that transforms in analogy with the QED gauge field A_μ.

Charged weak bosons $W^\pm$ which are experimentally observed, can be represented by the combination of the gauge fields W_1 *and* W_2 as

$$W_\pm^\mu = \frac{W_1^\mu \mp iW_2^\mu}{\sqrt{2}}. \tag{2. 16}$$

The photon and Z boson are the result of mixing the gauge fields W_3 and B_μ. To build up the final Lagrangian of the electroweak theory, one should keep in mind that fermions are arranged in left handed

weak isospin doublets and right handed singlets. So the local gauge invariant electroweak Lagrangian including all fermions and vector bosons is

$$L_{EW} = \underbrace{\sum_j i\overline{\psi_L^j}\gamma^\mu D_\mu^L \psi_L^j + \sum_{j,\sigma} i\overline{\psi_{R\sigma}^j}\gamma^\mu D_\mu^R \psi_{R\sigma}^j}_{E_{kin}\ fermions+interaction\ with\ gauge\ field} - \underbrace{\frac{1}{4}W_{\mu\nu}^a W_a^{\mu\nu}}_{E_{kin}\ gauge\ field} - \underbrace{\frac{1}{4}B_{\mu\nu}B^{\mu\nu}}_{gauge\ field\ self\ int} \tag{2.17}$$

where the index j represents different generations of fermions and the index σ represents up type and down type fermions respectively. As a consequence, a renormalizable local gauge invariant Lagrangian for electroweak interaction has obtained [1,6,7,13-16].

2.2.3 The Higgs mechanism

As we have seen in the previous section, in the GWS electroweak model, all the four gauge bosons and fermions are massless which is in contradiction of detected particles from experiments, moreover adding mass terms by hand would violate the gauge invariance, therefore a mechanism must exist to generate masses for gauge bosons and fermions while keeping photon massless and leaving the Lagrangian gauge invariant. The Higgs mechanism is a successful proposed theory for mass generation and is named after Peter Higgs, who developed this model in 1964 [17-19].

The idea of Higgs mechanism is based on the spontaneous symmetry breaking of the electroweak interaction which is the SU(2) × U(1) gauge symmetry. Consequently, the symmetry breaking will postulate existence of a scalar field, the Higgs boson, based on the Goldston theorem [20]. When other gauge bosons interact with the Higgs field, they become massive. In the following section, a simplified example of the spontaneous symmetry breaking followed by the Higgs mechanism is given to show how symmetry breaking can be used to obtain a massive gauge boson.

-Simple example of spontaneous symmetry breaking

As a first step to describe the symmetry breaking, a new complex scalar field needs to be defined as

$$\Phi = \frac{1}{2}(\Phi_1 + i\Phi_2). \tag{2.18}$$

With the local U(1) gauge invariant Lagrangian

$$L_{scalar} = (D^\mu\Phi)^\dagger \left(D_\mu\Phi\right) - V(\Phi) - \frac{1}{4}F_{\mu\nu}F^{\mu\nu}. \tag{2.19}$$

With $V(\Phi)=\mu^2(\Phi^\dagger\Phi) + \lambda(\Phi^\dagger\Phi)^2$ where $\lambda>0, \mu^2<0, D_\mu = \partial_\mu - ieA_\mu(x)$.

Now, we need to find out what are the implications of this new defined field on the Lagrangian and other particles. To do so, first, minimum of the defined potential should be fined. The minimum of the potential is called vacuum. In case of positive values for μ^2, the potential would have only a single trivial vacuum at $\binom{0}{0}$, which gives rise to two scalar massive particles φ_1 and φ_2 with mass μ. Although the exact symmetry of the Lagrangian is preserved in the vacuum and two massive scalar particles are generated, a desired gauge boson as the Higgs boson will not be produced. By choosing negative values for μ^2, the potential would have infinite number of vacua, each satisfying the $\Phi_1^2 + \Phi_2^2 = -\frac{\mu^2}{\lambda} = v^2$ relation, giving rise to a circle of vacua with radius $\sqrt{\frac{-\mu^2}{2\lambda}}$ as a minimum for the potential. The circle of vacua in this case,

does not preserve the symmetry of the Lagrangian, since a physical system, can only have one ground state, which means a single vacuum state. So the symmetry of the Lagrangian by choosing the negative values for μ^2 is spontaneously broken.

A convenient choice for a vacuum to have consistent physical outcomes that preserve symmetries and leads to desired gauge boson can be

$$\Phi_{1,vac} = \sqrt{\frac{-\mu^2}{2\lambda}} \equiv \frac{v}{\sqrt{2}} \text{ and } \Phi_{2,vac} = 0. \tag{2.20}$$

Where v is called the vacuum expectation value.

This proposed vacuum has a transformation of $\Phi(x) \rightarrow \Phi'(x) = e^{-i\alpha(x)}\,\Phi(x)$ under the $\mathrm{U}(1)$ while leaving the Lagrangian invariant. As we will see, the existence of a non-vanishing vacuum expectation value is the key point for mass generation of the gauge bosons.

To express the Lagrangian in terms of the new introduced field, it is useful to look at a small perturbation around the minimum of the potential which can be expressed by adding small shift fields η and z to the minimum as

$$\Phi = \frac{1}{\sqrt{2}}(\eta + v + i\zeta\,) \tag{2.21}$$

and the Lagrangian in terms of the perturbed field would be

$$L(\eta,\zeta) = \underbrace{\frac{1}{2}(\partial_\mu\eta)^2 - \lambda v^2\eta^2}_{\eta-particle} + \underbrace{\frac{1}{2}(\partial_\mu\zeta)^2}_{\zeta-particle} - \underbrace{\frac{1}{4}F_{\mu v}F^{\mu v}}_{photon\ field} + \underbrace{\frac{1}{2}e^2v^2A_\mu^2}_{photon\ field} - \underbrace{evA_\mu(\partial^\mu\zeta)}_{unknown} + \text{int.terms} \tag{2.22}$$

So far we added a complex scalar field which has brought two degrees of freedom to the existing Lagrangian and has broken its symmetry. Those additional degrees of freedoms lead to mass terms for gauges bosons that are related to broken symmetries.

In the obtained Lagrangian, beside the A_μ which is the gauge boson, two other scalar particles are described, a massive η-particle with mass of $\sqrt{-\mu^2}$ and the massless z particle which is called the Goldstone boson that is generated based on the Goldstone theorem which says for every broken generator of the symmetry , an associated massless scalar particle would be produced. The η-particle which is scalar, can be interpreted as the Higgs boson.

The defined Lagrangian above, contains a term proportional to A_μ^2 with the generated mass of ev. This term can be interpreted as the general expression for the massive gauge bosons in the form of $\frac{1}{2}M_V^2 v^\mu v_\mu$.

The Lagrangian contains an unknown term as well which can be omitted by re-writing the Lagrangian in the unitary gauge transformation by taking the advantage of the gauge freedom of A_μ as

$$A_\mu \rightarrow A_\mu' = A_\mu - \frac{1}{ev}(\partial_\mu\zeta). \tag{2.22}$$

and applying the local phase transformation as well, which leads to a real scalar field as

$$\Phi \rightarrow \Phi' = e^{-i\zeta(x)/v}\Phi = \frac{v+\eta}{\sqrt{2}}. \tag{2.23}$$

And if we represent η by h, the real scalar Higgs field, we have

$$\Phi' = \frac{v+h}{\sqrt{2}}. \tag{2.24}$$

by rewriting the Lagrangian in terms of the real scalar field, which is yielded from the local phase transformation of the primary complex scalar field, it can be seen the obtained Lagrangian, is gauge invariant.

$$L_{scalar} = \underbrace{\frac{1}{2}(\partial_\mu h)^2 - \lambda v^2 h^2}_{E_{kin}\ and\ mass\ term\ of\ Higgs} - \underbrace{\frac{1}{2}e^2 v^2 A_\mu^2 + \frac{1}{4}F_{\mu\nu}F^{\mu\nu}}_{mass\ term\ of\ the\ gauge\ boson\ and\ E_{kin}} + \underbrace{e^2 v A_\mu^2 + \frac{1}{2}e^2 A_\mu^2 h^2}_{interaction\ of\ Higgs\ and\ gauge\ field} - \underbrace{\lambda v h^3 - \frac{1}{4}\lambda h^4}_{Higgs\ self\ interaction} \tag{2.25}$$

To sum up, the introduction of a complex scalar field with non-vanishing expectation value for vacuum leads to spontaneous symmetry breaking which generate mass terms for gauge bosons. More over a real scalar massive gauge boson has appeared which can be interpreted as the Higgs boson.[1,6,7 &21].

-The Higgs mechanism in $\mathbf{SU(2)_L \times U(1)_L}$

To build the Higgs mechanism in the standard model, the $SU(2)_L \times U(1)_L$ symmetry needs to be broken spontaneously to generate mass for three gauge bosons, $W^-, W^+,\ Z^0$ while leaving the photon massless. Moreover this mechanism generates mass for fermions as well.

To break the $SU(2)_L \times U(1)_L$ symmetry, an isospin doublet with hypercharge Y=1 and weak isospin I=$\frac{1}{2}$ with four degrees of freedom should be defined as

$$\Phi = \begin{pmatrix} \Phi^+ \\ \Phi^0 \end{pmatrix} = \frac{1}{\sqrt{2}} \begin{pmatrix} \Phi_1 + i\Phi_2 \\ \Phi_3 + i\Phi_4 \end{pmatrix}. \tag{2.26}$$

The local gauge invariant Lagrangian for this doublet is

$$L_{scalar} = (D^\mu \Phi)^\dagger (D_\mu \Phi) - V(\Phi). \tag{2.27}$$

Where $V(\Phi) = \mu^2(\Phi^\dagger \Phi) + \lambda(\Phi^\dagger \Phi)^2$ with $\mu^2 < 0$, and

$$D_\mu = \partial_\mu + ig\frac{1}{2}\vec{\tau}.\overrightarrow{W_\mu} + ig'\frac{1}{2}YB_\mu \tag{2.28}$$

In this Lagrangian only the left handed doublet with I=½ is added.

As we have seen in the previous case, for μ^2<0, the potential would have infinite number of vacua, so it does not preserve the symmetry of the Lagrangian. A convenient choice for a physical vacuum state would be $\Phi_1 = \Phi_2 = \Phi_4 = 0$ and $\Phi_3 = \frac{v}{\sqrt{2}}$ so the vacuum can be defined as $< \Phi >_0 = \begin{pmatrix} 0 \\ v/\sqrt{2} \end{pmatrix}$. With this selected vacuum, the symmetry $SU(2)_L \times U(1)_Y$ is broken, but $U(1)_{EM}$ is preserved which means the photon will remain massless. As we have seen for the previous case, small perturbations need to be added to the minimum of the potential to find out which new particles would be generated by this new potential, the small perturbations can be represented by three real fields ζ^i and one real field η as

$$\Phi = e^{\frac{i\zeta^i \tau_i}{2v}} \begin{pmatrix} 0 \\ v + \eta/\sqrt{2} \end{pmatrix}. \tag{2.29}$$

writing the Lagrangian for this new perturbed filed will give rise to four particles, three ζ^i particles which are massless and don't have physical interpretation and a η field which is massive. It is always possible to find a suitable unitary gauge transformation to rotate away the ζ^i fields and represent the perturbation around the vacuum as;

$$\Phi = \begin{pmatrix} 0 \\ v+\eta/\sqrt{2} \end{pmatrix}. \tag{2.30}$$

To build the Lagrangian which is invariant under unitary gauge transformation, this new field should be replaced in $L_{scalar} = (D^{\mu}\Phi)^{\dagger}(D_{\mu}\Phi) - V(\Phi)$ where η is replaced by scalar Higgs field h and the covariant derivative of the form

$$D_{\mu}\Phi = \partial_{\mu} + ig\frac{1}{2}\vec{\tau}.\overrightarrow{W_{\mu}} + ig'\frac{1}{2}YB_{\mu}\left[\begin{pmatrix} 0 \\ v+h/\sqrt{2} \end{pmatrix}\right]. \tag{2.31}$$

As it is shown in the previous section, the mass terms for gauge bosons are proportional to v^2 and their interaction with the Higgs field is proportional to vh or h^2, to be more focused on the mass terms, only the part proportional to v^2 is written explicitly as below

$$(D^{\mu}\Phi)^{\dagger}(D_{\mu}\Phi)=\left[\left(-i\frac{g}{2}(\tau_1 W_1 + \tau_2 W_2 + \tau_3 W_3) - i\frac{g'}{2}B_{\mu}\right)\begin{pmatrix} 0 \\ \frac{v}{\sqrt{2}} \end{pmatrix}\right]^2. \tag{2.32}$$

and if replace W_1 *and* W_2 by $W^{\pm} = \frac{W_1 \mp W_2}{\sqrt{2}}$

The equation can be simplified to

$$(D^{\mu}\Phi)^{\dagger}(D_{\mu}\Phi) = \left(\frac{1}{2}vg\right)^2 W_{\mu}^{+}W^{-\mu} + \frac{1}{8}v^2(W_{\mu}^{3}, B_{\mu})\begin{pmatrix} g^2 & -gg' \\ -gg' & g'^2 \end{pmatrix}\begin{pmatrix} W^{3\mu} \\ B^{\mu} \end{pmatrix}. \tag{2.33}$$

In fact $W^{\pm}$ represent the electroweak force mediator, W^{-}*and* W^{+}, with the mass term

$$m_w = \frac{1}{2}\, gv\,. \tag{2.34}$$

moreover by mixing of W_3 and B_{μ}, the fields A_{μ} *and* Z_{μ} , corresponding to the photon and Z boson can be made as

$$Z_{\mu} = \cos\theta_W\, W_{\mu}^{3} - \sin\theta_w\, B_{\mu} \tag{3.35}$$

$$A_{\mu} = \sin\theta_w\, W_{\mu}^{3} + \cos\theta_w\, B_{\mu}$$

where θ_w called Weinberg angle and their mass is can be calculated by diagonalizing the matrix below

$$\mathrm{M}=\begin{pmatrix} g^2 & -gg' \\ -gg' & g'^2 \end{pmatrix}. \tag{2.36}$$

This matrix has two Eigen values, λ =0 and λ = ($g^2 + g'^2$), the zero Eigen value corresponds to $\frac{1}{\sqrt{g^2+g'^2}}(g'W_3+gB_{\mu}) = A_{\mu}$ which represents the photon field with mass zero and the other Eigen value corresponds to $\frac{1}{\sqrt{g^2+g'^2}}(g\ \ W_3+g'B_{\mu}) = Z_{\mu}$ which represent the Z-boson field with mass $m_z = \frac{1}{2}v\sqrt{g^2 + g'^2}$

Now it is possible to re-write the covariant derivative in terms of the physical fields:

$$D_{\mu} = \partial_{\mu} + i\frac{g}{\sqrt{2}}(\tau^{+}W_{\mu}^{+} + \tau^{-}W_{\mu}^{-}) + i\frac{g}{\cos\theta_w}(\tau_3 + \sin\theta_w{}^2\, Q)Z_{\mu} + ieQA_{\mu}. \tag{2.37}$$

In brief, by introducing the complex Higgs field with four degrees of freedom with non-vanishing vacuum expectation value, the $\mathrm{SU(2)_L} \times \mathrm{U(1)_Y}$ symmetry of the system is broken and consequently, three massive gauge bosons, the $W^{\pm}$ *and* Z^0 bosons and one massless photon are generated followed by gen-

eration of a massive scalar particle which is called the Higgs boson. The next step to obtain a full Lagrangian in the SM that describes all the particles would be generating mass terms for fermions. In the Dirac Lagrangian, the general expression for a fermion mass term is $m\bar{\psi}\psi$, which is not gauge invariant, pointing out that fermions are treated differently under the weak interaction based on their chirality, the left handed fermions transform as an isospin doublet, while the right handed fields transform as an isospin singlet, thus the mass term would break the gauge invariance of the Lagrangian because it mixes a right handed fermion with a left handed fermion term. To write a mass term which is invariant under $SU(2)_L \times U(1)_Y$ rotation transformation, it should transform as an isospin singlet under $SU(2)_L$ as well as$U(1)_Y$. This can be achieved by the introduced complex Higgs filed, since the Higgs field has both required quantum numbers to construct fermion mass terms which are singlet under both $SU(2)_L$ and $U(1)_Y$. For the coupling of the Higgs field to fermions we have

$$\lambda_f \overline{\psi_L} \Phi \psi_R \,. \tag{2.38}$$

which is called Yukawa coupling.[18]

The introduced Yukawa coupling would allow a mass term in the SM Lagrangian which shows the coupling of the Higgs doublet to the fermion field as

$$L_{fermion-mass} = -\lambda_f [\overline{\psi_L}\, \Phi \psi_R + \overline{\psi_R} \Phi \overline{\psi_L}]. \tag{2.39}$$

with mass of $m_f = \frac{\lambda_f v}{\sqrt{2}}$, which describes the mass terms for fermions as well as the interaction term with the Higgs field. It can be check that the mass terms are a singlet under U(1) as well as SU(2) rotation. As a result, the mixing of left and right handed states will not occur and the expression for the mass term will be gauge invariant. If we represent λ_f by G_f which is called Yukawa coupling, the Yukawa Lagrangian that contains mass terms for both leptons and quarks can be written as

$$L_{Yukawa} = -\, G_l^{ij} \overline{L_L^i} \Phi l_R^j \; - G_d^{ij}\, Q_L^{-i} \Phi d_R^j - G_u^{ij} Q_L^{-i} i\sigma_2 \Phi^* u_R^j + \text{h .c.} \tag{2.40}$$

where fields $Q_L^i = (u, d)$ and $L_L^i = (v_l, l)$ represents quarks and lepton doublets respectively. As the result, the complete SM Lagrangian can be expressed as

$$L_{SM} = \underbrace{-\frac{1}{4} B^{\mu v} B_{\mu v} \; - \frac{1}{4} W^{i\mu v} W_{i\mu v} \; - \frac{1}{4} G^{a\mu v} G_{a\mu v}}_{gauge\ bosons} +$$

$$\underbrace{\overline{\psi_L} \gamma^\mu D_\mu \psi_L}_{EW\ left\ handed\ quarks\ or\ leptons} \quad + \quad \underbrace{\overline{\psi_R} \gamma^\mu \left(i\partial_\mu + g_Y \frac{Y}{2} B_\mu \right) \psi_R}_{EW\ right\ handed\ quark\ and\ leptons} \quad + \tag{2.41}$$

$$\underbrace{\bar{q}\, \gamma^\mu \left(i\partial_\mu - gsTG_\mu \right) q}_{QCD\ interaction\ of\ quarks\ and\ glouns} \quad + \underbrace{|D_\mu \Phi|^2 - \mu^2 (\Phi^+ \Phi) - \lambda (\Phi^+ \Phi)^2}_{Higgs\ potential} \underbrace{-g_l \bar{L}\, \Phi R - g_d \bar{Q} \Phi d_R - g_u \bar{Q} \Phi_c u_R}_{Yukawa\ terms}$$

More details about the Higgs mechanism in the SM are given in [1,6,7, 21,22].

2.2.4 Properties of the SM Higgs boson

The mass term, the self-coupling and the properties of Higgs boson can be determined by the Higgs Lagrangian terms as;

$$L_H = \frac{1}{2}\left(\partial_\mu H)(\partial^\mu H) - V(H\right) = \frac{1}{2}(\partial_\mu H)^2 - \lambda v^2 H^2 - \lambda v H^3 - \frac{1}{4}\lambda H^4 \tag{2.42}$$

where the mass term is $m_H = 2\lambda v^2 = -2\mu^2$ and $v = \frac{2m_w}{g_2} = 246$ GeV. It can be seen the Higgs boson has the triple and quadratic self-interaction terms proportional to

$$g_{HHH} \propto \frac{m_H^2}{v}. \qquad g_{HHHH} \propto \frac{m_H^2}{v^2}.$$

The SM has predicted some properties of Higgs boson, like its quantum numbers but its mass and some parameter of the Higgs potential are not specified. Some theories in the SM have provided limitations for its mass, but determining the exact mass is not possible without experiment. Many experimental groups at LEP, Tevatron [20] and the LHC, had carried experiments to measure the mass of the Higgs boson. Finally in the summer 2012, both ATLAS and CMS at the LHC, confirmed observation of a particle with the mass range in agreement with the Higgs boson and the combined result of both experiments, has set the mass of Higgs boson to 125±0.3 GeV [23,24]. The observed SM Higgs boson is electrically neutral, positive parity, with spin zero.

-The Higgs production channels

The Higgs boson can be produced through different mechanisms at the LHC. Here the list of these mechanisms which are ordered by production cross section is given. The gluon gluon fusion production through a top quark loop process ($gg \rightarrow h$) [25], the vector boson fusion production process ($qq \rightarrow qqh$) [26], Higgs strahlung process ($qq \rightarrow WH, ZH$) [27] and production in association with heavy top or bottom quark pair ($qq/gg \rightarrow t\bar{t}H, b\bar{b}H$) [28].

Figure 6, shows the leading order Feynman diagrams of all the Higgs production channels. The gluon gluon fusion (ggF) production channel is mostly mediated by top quark loop. This process is directed by strong interaction and is the dominant channel with the highest production cross section because of the large coupling of the Higgs boson to top quark. This production cross section is an order of magnitude larger than the second largest one, vector boson fusion (VBF) production mechanism. The GGF mechanism is interesting as it can be studied to extract the CP properties of the top Yukawa coupling and the effective coupling of Higgs to gluon through top loop [29-30]. The VBF process is directed by electroweak interaction because Higgs boson is produced by the quark scattering which is mediated by a weak gauge boson. The scattered quarks can become two energetic jets. This channel has a clear signature so it can be a good candidate to study the signal signature. This process also provides a proof that the Higgs mechanism is the source of EW symmetry breaking and is suitable for extracting the strength of the Higgs boson coupling to vector bosons. The Higgs Strahlung process which is referred as associated production with a vector boson (VH), is kinematicaly suppressed, because in order to create a vector boson aside a Higgs boson, high energy is required, so this process has low production cross section [1]. The associated production with top quark pair has the lowest cross section because the initial gluons need

to have very high momenta in order to produce top quark pair and Higgs boson. Figure 7, shows the production cross section of the SM Higgs boson as a function of its mass at a center- of- mass energy of 14 TeV [31].

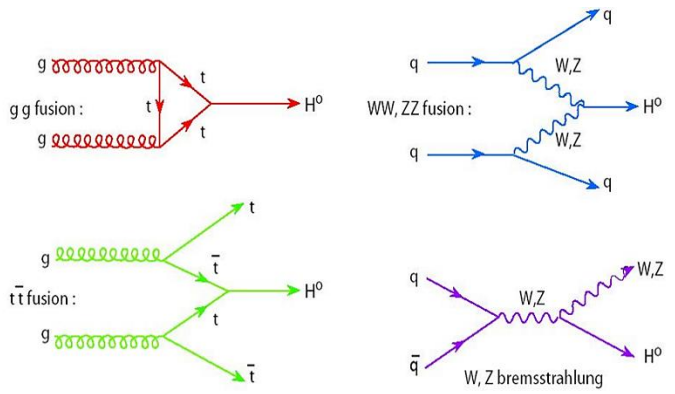

Figure 6. The Feynman diagrams of Higgs production at leading order.

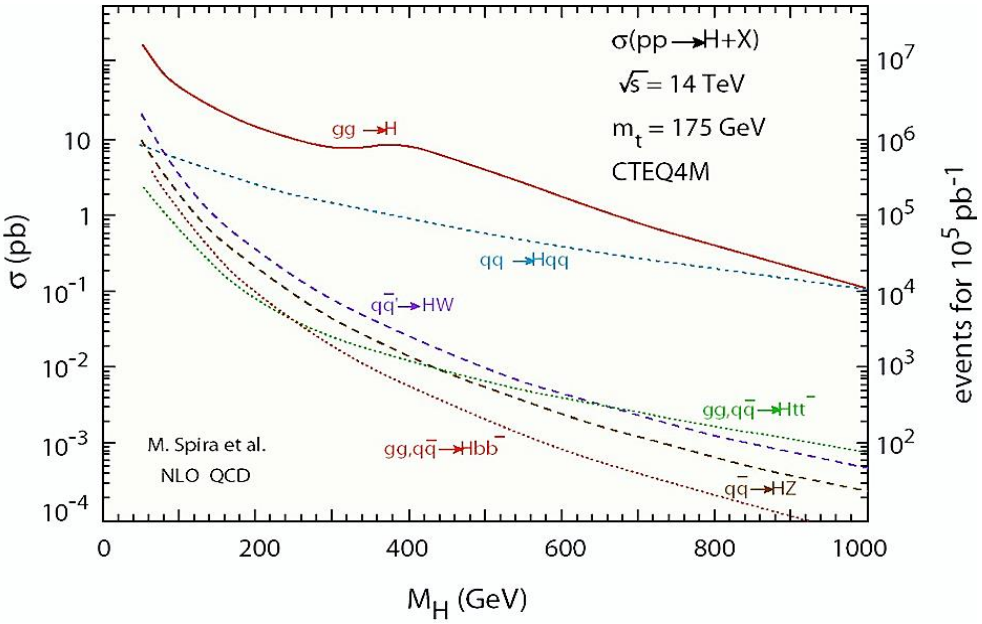

Figure 7. The cross section of Higgs Boson production at the LHC at the center of mass energy of 13 TeV.

-The Higgs boson decay channels

Higgs boson decays almost immediately after being produced. The average life time of Higgs boson for m_H=125 GeV is 10^{-22} s [7]. As the Higgs boson couples to all the massive particles, its decay process can have many different final states. It can decay to a pair of leptons, quarks, weak gauge bosons, gluons, photons or a photon and a Z boson. Figure 8.a, shows the branching ratios for each decay channel and figure 8.b, shows the total decay width of the Higgs boson [31].

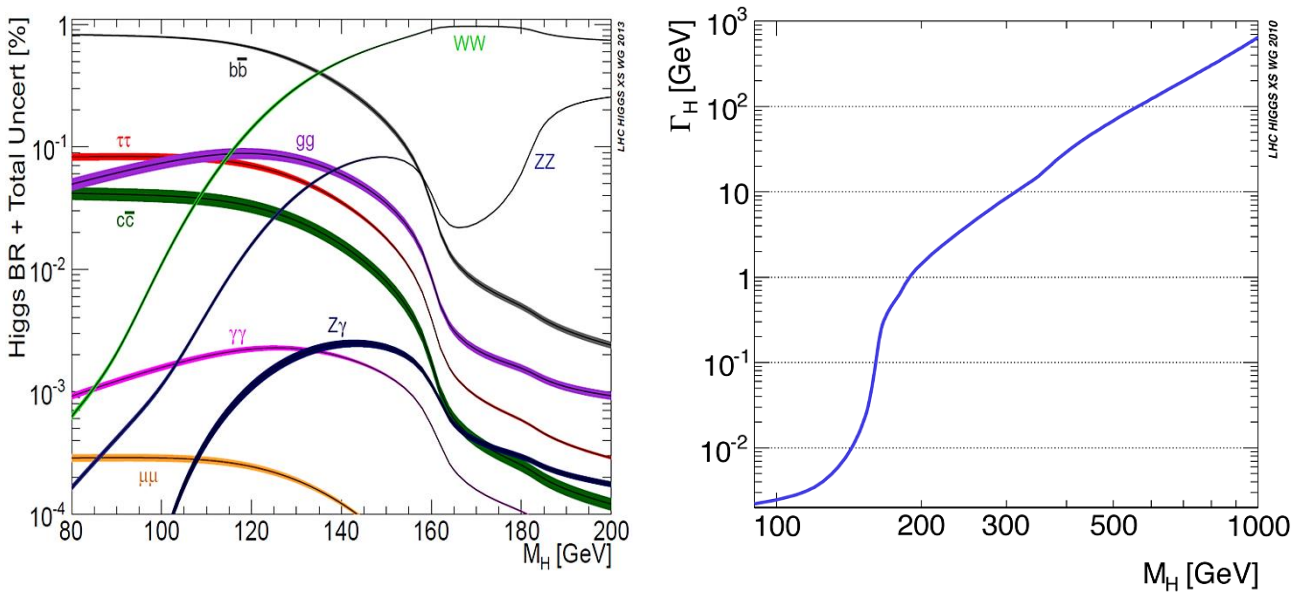

Figure 8. Different Higgs boson decay channle branching ration on the left and the total decay width of the Higgs boson on the right for 13 TeV

2.3 The Higgs boson beyond the SM

This section will review the Higgs boson extension beyond the Standard Model.

As the subject of this thesis is studying the CP properties of the Higgs boson which is produced through the vector boson fusion channel and through the gluon gluon fusion channel, the theoretical overviews of the Higgs boson will be more focused on the coupling of Higgs boson with gluons and vector bosons and the properties of these couplings beyond the Standard Model.

2.3.1 Why beyond the SM

Although the Standard Model of the particles is an elegant theory which gives descriptions of the particles and their interactions based on symmetries of the nature, it has some unsolved problems and some inconsistencies with experimental results. For instance it cannot explain gravity, dark matter, matter antimatter asymmetry, strong CP problems or the existence of more than one Higgs bosons and many more questions.

To overcome the Standard Model problems, there are some theories beyond the Standard Model (BSM) that propose solutions but there is no experimental evidence yet.

Some of the theories in BSM, are considered as extensions of the SM, such as the Minimal Supersymmetric Standard Model (MSSM) or extensions of the Higgs sector, also some of them are quite innovative, such as string theory and extra dimensions [1,32].

In the next section a short review of the extensions of the SM Higgs boson to beyond the SM are given.

2.3.2 Higgs boson extension

After discovery of the Higgs boson in 2012, there is a crucial question whether the discovered particle is the only Higgs boson that exists in nature or is there a possibility to have extensions or more new

Higgs boson type particles. Existence of a new Higgs boson or extension of the scalar sector may introduce different properties or quantum numbers for the Higgs boson, rare or new decays or different couplings respect to the SM that can lead to a solution some unsolved problems of physics such as dark matter or matter anti-matter asymmetry [1,32].

Since the subject of this thesis is CP violation in the Higgs production sector, the relation of the BSM Higgs boson to the matter-antimatter imbalance in the Universe becomes interesting. Based on expectation from theories, after the Big Bang, the amount of produced anti-matter was the same as matter, but experimental results have shown the amount of observed matter is more than anti matter. So there must be some physical processes that have caused the imbalance between matter and anti-matter.

There are some possible explanations for this problem in SM, for instance CP violation in weak interaction which originates from the CKM matrix [33], but the amount of asymmetry that is predicted by this theory is very less than the observed one, so there must be some other sources of CP violation in nature that explain the asymmetry.

CP violation in the Higgs sector could be a good candidate to resolve this problem by introducing a new Higgs boson coupling beyond the standard model which is a CP-odd coupling or an extension for CP-even coupling. The existence of a new coupling could allow new types of interactions where the CP-symmetry is not conserved.

There are some models that introduce the extension of the SM Higgs boson to beyond the standard model, for instance Minimal Composite Higgs Model which proposes that the light Higgs boson being a composite pseudo Nambu-Goldstone boson , instead of an elementary particle, or Additional Electro Weak single which states, addition of a real scalar filed X which transforms as singlet under the SM gauge group and can be a possible candidate to dark matter problem or the Two Higgs Doublet Model which is constructed by adding a second complex double of scalar field with weak hyper charge-1 to the scalar sector of SM, this model can incorporate in CP violation in Higgs sector [32].

2.3.3 Effective field theory

To study physical models beyond the SM, since often there is not enough information to give a description about a physical problem, theories with new model dependent free are proposed. Often, developing a BSM theory, starts by assuming a certain energy scale where a transition from SM to BSM appears and the effects of BSM become more pronounced. Then, new terms, new free parameters and dynamical degrees of freedom need to be added to the SM Lagrangian which preserve the required symmetries. These new parameters depend on the energy scale and cutoff scale which experimental results can provide limits on them.

To study the CP violation in the Higgs production, a BSM extension of Higgs boson which allows different couplings with different CP properties is needed. The Higgs characterization Model which is described in detail in [34,35], introduces an appropriate effective theory to describe the BSM extension with inclusion of both CP-even and CP-odd couplings for the Higgs boson.

The next section gives the effective Lagrangian related to the Higgs coupling to gluons and vector bosons.

2.3.4 Effective Lagrangian for Higgs production through gluon gluon fusion channel

The most vigorous way to start building an effective Lagrangian is first applying all the SM symmetries, for instance starting from electroweak symmetry and adding higher dimensional operators, Higgs boson does not couple to gluons directly, usually it couples through the top quark loop, as the Feynman diagram in figure 3 shows.

The effective Lagrangian for coupling of Higgs to top quark through induced loop is [35];

$$L_Y^t = -\overline{\psi_t}\,(c_\alpha k_{Htt} g_{Htt})\psi_t H - \overline{\psi_t}(i s_\alpha k_{Att} g_{Att}\gamma_5)\psi_t A. \tag{243}$$

which shows the effective top Yukawa coupling. In this Lagrangian the possibility of both scalar and pseudo-scalar couplings, i.e. CP-odd and CP-even couplings for the Higgs boson is assumed where $c_\alpha = \cos\alpha$ represents the SM CP-even case and $s_\alpha = \sin\alpha$ represents the CP-odd case. k_{Htt} and k_{Att} are dimentionless real coupling parameters and g_{Htt}=g_{Att}=$\frac{m_t}{v}$..

The Higgs interaction with gluons which is top loop induced can be represented as;[34]

$$L_{Hgg}^{loop} = -\frac{1}{4}\left[\underbrace{c_\alpha k_{Hgg} g_{Hgg} G_{\mu\nu}^a G^{a,\mu\nu}}_{with\ CP-even\ coupling}\right] H - \frac{1}{4}\left[\underbrace{s_\alpha k_{Agg} g_{Agg} G_{\mu\nu}^a \tilde{G}^{a,\mu\nu}}_{with\ CP-odd\ coupling}\right] A\,. \tag{2.44}$$

where $G_{\mu\nu}^a = \partial_\mu G_\nu^a - \partial_\nu G_\mu^a + g_s f^{abc} G_\mu^b G_\nu^c$ represents the gluon strength tensor and $g_{Hgg} = -\frac{\alpha_S}{3\pi v}$ $g_{Agg} = \frac{\alpha_s}{2\pi v}$.

When $c_\alpha = 1$, the Lagrangian represents the pure CP-even standard model case which corresponds to couplings to fermions as are described in the SM. $s_\alpha = 1$, represents the CP-odd case which is BSM and it corresponds to pure pseudo scalar state. If $c_\alpha = s_\alpha = \frac{1}{\sqrt{2}}$ it represents the CP-mixed state where the spin zero Higgs boson is in the superposition of scalar and pseudo scalar state.

It is also common to represent the Lagrangian in equation (2.44) as [29]:

$$L_{Hgg}^{loop} = a_2 G_{\mu\nu}^a G^{a,\mu\nu} H + a_3 G_{\mu\nu}^a \tilde{G}^{a,\mu\nu} A\,. \tag{2.45}$$

where a_i is scalar form factor and can be represented as;

$$a_2 = -\frac{1}{4} c_\alpha k_{Hgg} g_{Hgg} \ \text{ and } \ a_3 = -\frac{1}{4} s_\alpha k_{Agg} g_{Agg} \tag{2.46}$$

and they correspond to the CP-even and CP-odd couplings respectively.

The effective tenor structure for Hgg vertex which is obtained from this Lagrangian, can be written as:

$$T^{\mu\nu} = a_2\left(q_1 \cdot q_2 g^{\mu\nu} - q_1^\nu q_2^\mu\right) + \ a_3 \varepsilon^{\mu\nu\rho\sigma} q_{1\sigma} q_{2\sigma}\,. \tag{2.47}$$

Where $q_{1\sigma}$ and $q_{2\sigma}$ are the four momenta of the incoming gluons and $P_1$and P_2 are the three momenta of the incoming gluons.

Writing tensor structure and effective Lagrangian in the form of equations (2.45) and (2.47) is useful for constructing CP-sensitive observable for analysis which will be explained in the next chapter.

In this notation for the pure CP-even in the SM we have: $a_2 = \ k_{Hgg} = 1, a_3 = k_{Agg} = 0$ and for pure CP-odd case we have: $a_2 = k_{Hgg} = 0, a_3 = k_{Agg} = 1$.

More details about the Higgs effective Lagrangian are given in [29,30,34,35].

2.3.5 The effective Lagrangian for Higgs production th

2.3.6 rough vector boson fusion channel

The effective Lagrangian for Higgs boson coupling to massive gauge bosons, in our case W boson, can be written as [34]:

$$L_0^W = \{c_\alpha k_{SM}\left[g_{HWW} W_\mu^+ W^{+\mu}\right] - \left[\frac{1}{2}\frac{1}{\Lambda} c_\alpha k_{HWW} W_{\mu\nu} W^{-\mu\nu} + \frac{1}{2}\frac{1}{\Lambda} s_\alpha k_{AWW} W_{\mu\nu}^+ \widetilde{W^{-\mu\nu}}\right] - \frac{1}{\Lambda} c_\alpha [\left(k_{H\partial W} W_\nu^+ \partial_\mu \widetilde{W^{-\mu\nu}} + h.c\right)]\} X_0 \quad (2.48)$$

where $g_{HWW} = 2\frac{m_W^2}{v}$ is the SM coupling and Λ is the cutoff scale where the BSM effects become important. In the construction of the effective Lagrangian for VBF channel, a possibility for extension of CP-even coupling in BSM aside CP-odd is also considered which their effect depend on the cutoff scale. In this Lagrangian the first term shows the SM CP-even coupling to the W boson when $c_\alpha = k_{SM} = 1$. The second and the forth terms represent the extension of the Higgs CP-even coupling to BSM. When $k_{SM} = 0$ *and* $c_\alpha = k_{HWW} = k_{H\partial W} = 1$, it represents the BSM CP even coupling.

If $k_{AWW} = 1$and $s_\alpha = 1$ and $c_\alpha = 0$, represents the pure CP-odd coupling in BSM. When $s_\alpha = \frac{1}{\sqrt{2}}$ and $c_\alpha = \frac{1}{\sqrt{2}}$, it represents a mixed scalar pseudo scalar state.

The tensor structure of the HVV vertex can be represented as

$$T^{\mu\nu}(q_1, q_2) = a_1(q_1, q_2) g^{\mu\nu} + a_2(q_1, q_2)\left[q_1 . q_2 g^{\mu\nu} - q_2^\mu q_1^\nu\right] + a_3(q_1, q_2)\varepsilon^{\mu\nu\rho\sigma} q_{1\rho} q_{2\sigma} \quad (2.49)$$

where first tem with a_1 is the SM CP-even coupling, the second term with a_2 is the BSM CP-even coupling and the third term with a_3 is the BSM CP-odd coupling. $q_{1\sigma}$ and $q_{2\sigma}$ are the four momenta of the incoming vector bosons and $P_1$and P_2 are the three momenta of the vector bosons.

More details about the Higgs effective Lagrangian are explained in [34,36].

3 ANALYSIS AND RESULTS

After the theoretical review of the Higgs boson phenomenon, its properties in the Standard Model and definition of the effective Lagrangian of the BSM Higgs boson, we are ready to describe the analysis. In the analysis, the CP nature of the Higgs boson coupling is measured which is produced through gluon gluon fusion and vector boson fusion channel with two tag jets. The goal of this chapter is first to review the analysis setup, then describing the research followed by interpretation of the results.

Before going through the analysis description, it is necessary to give a brief introduction to event generation and a discussion on the settings of the Monte Carlo generator used to generate simulated signal samples followed by event selection.

3.1 Event generation and simulations

In order to model the real collision data and compare it with theoretical predictions, event samples need to be simulated. The simulation consist of two parts: Physical process simulation and detector simulation. For this means, different event generators and programs can be used. Monte Carlo (MC) generator is an important event generator in physics which produces events based on physical models. As we know, in particle physics, only the probability of the occurrence of a certain final state can be determined, the Monte Carlo technique uses these probabilities, which are the production cross section of the process under the study, to generate interaction between the incoming partons (gluon, quarks) and final state decay products. In the first step of the simulation, the proton- proton collision at the LHC is generated and large event samples are made based on a chosen physical model for the process of under the study, then, they can be passed into the detector simulation to model precisely the real environment of the experimental setup. Once the events are simulated, in order to do the full analysis, each event should be reconstructed from the final state particles which are detected and measured based on the trace of the electric signals they leave in the detector. The event reconstruction can be done by different algorithms to define the physical objects produced in each event [1].

3.2 Analysis setup

To study the CP properties of the top Yukawa coupling in ggF channel, the signal samples for Higgs production in association with two energetic jets is generated and the possibility for both CP-even and CP-odd couplings to top quark is included. To study the tensor structure of the HWW vertex, the signal for VBF production mechanism is generated by Higgs production from quark scattering and theses quarks become energetic jets subsequently. Small VH contribution is also added to the VBF signal and the possibility of both scalar and pseudo-scalar couplings to vector boson is considered. In both production

mechanisms, the Higgs boson is decayed into W pair and then W pair is decayed leptonically, the azimuthal angle is studied at next to the leading order in QCD including the parton shower effect at the center of mass energy of 13 TeV for M_h=125 GeV for proton proton collision at the LHC. A brief review of generator setting is given here.

3.2.1 Hard scatter simulation

In the first step, the hard scatter simulation is done with MadGraph based on the Higgs Characterization model that is discussed in the theory chapter, then the matrix element is calculated based on the effective Lagrangian for our process which is spin-0 Higgs boson production in association with two energetic jets in ggF and VBF channel by considering the existence of both Hjj scalar and Ajj pseudo scalar couplings. In matrix element calculations, the NLO-QCD corrections are included by MC@NLO and the total cross section is calculated with NLO precision. Then the parton distribution functions are calculated.

3.2.2 Parton showering

The modelling of the parton shower, hadronization and the underlying events are done by PYTHIA 8. The MadGraph parton level generated processes are passed to PS to become showered, the hadronization starts when the energies of particles are in the order of 1GeV where the branching of the quarks and gluons ends. The decay of Higgs boson to W boson pair is modelled including the decay of W pair into four leptons in both ggF and VBF samples. For VBF samples, the VH mechanism is modelled with PYTHIA 8 as well.

3.2.3 Event reconstruction and event selection

Most interesting particles that are created in hard scatter processes, decay before being detected, so the ATLAS detector only measures the decay products. On the other hand, some other processes that come from proton proton collision and the detector noise, form background to Higgs boson production mechanism with two jets signals. To be able to do the full analysis, first, each event should be reconstructed from the final state particles which are detected and measured based on the trace of the electric signals they leave in the detector. Then, after reconstruction and identification of all relevant final state objects, signals must be identified from background. One of the most important and challenging tasks in particle physics analysis is enhancing the signal over the background ratio by improving the trigger system and finding the optimal selection criteria. So we need to find a specific set of cuts to suppress the background and enhance the significance of signal region. First, some kinematic cuts as pre-selection criteria or acceptance cuts are applied to include detector acceptance and remove background to obtain significant signal region. These cuts confirm that two tagging jets and two leptons in our case are observed inside the detector and well separated from each other for each event. Then the ggF and VBF events selection cuts are applied followed by the CP discriminating cuts.

Event selection in ggF:

In this channel, the signal is characterized by Higgs production with two energetic jets with the subsequent decay of Higgs into to W pair which decay leptonically. The tagged jets are the two jets with the highest momentum in each event, so a cut on transverse momentum of the jets is required to select the signal topology. Moreover, rapidity of jets must be less than 4.5 to guarantee they are detected in the hadronic calorimeter. In this analysis only the signal samples as well as the signal signatures are studied. In the real data, background to this production channel is expected, so it is important to have the signal signature to reduce the background and enhance the signal significance. The main physical background to oppositely charged leptons and energetic jets signal is from $t\bar{t}$ + jet production followed by top quark decay to b-quark which emerges as tagging jets. To reduce this background, it is necessary to use b-veto to reject all the events that contain b jets as the tag jets. The background studies are done with details in [1].

Table 1, shows the list of the acceptance and ggF signal selection cuts. Table 2, gives the number of events (signal) that passed the applied cuts as well as the expected number of events for the Higgs production with two jets in ggF channel with the subsequent decay of the Higgs boson to W boson pair, that has a cross section of 0.022 pb for the give luminosity of 300 fb^{-1} [34].

ggF EVENT SELECTION	
Acceptance cuts	$n_j \geq 2$ $P_j^T \geq 20\ GeV$ $\lvert\eta_j\rvert \leq 4.5$
$H \rightarrow WW^* \rightarrow lvlv$ topology	Two opposite charged and opposite flavor leptons, $P_{llep}^T \geq 20\ GeV$, $P_{sublep}^T \geq 10\ GeV$ $\lvert\eta_{lep}\rvert \leq 2.5, \lvert\eta_{sublep}\rvert \leq 2.5$ $M_{ll} \geq 10\ GeV$ $\lvert\Delta\varphi_{ll}\rvert \leq 1.8$ $MET \geq 20\ GeV$

Table 1. Event selection criteria for the Higgs production in ggF associated with two tagged jets.

Cut	***MC CP-ODD***	***MC CP-EVEN***	***Expected number of events for SM Higgs boson***
Acceptance cut	*187856*	*191030*	*1200*
All cuts	*83670*	*84968*	*535.4*

Table 2. Shows the number of events after applied acceptance cuts and after all applied cuts.

Event selection in VBF:

To select the VBF signal topology, events with 2 isolated leptons and energetic jets are needed. Leptons are required to have opposite electric charge. The transverse momentum of the leading leptons must be greater than 20 GeV, for the sub leading lepton must be greater than 10 GeV with the invariant mass of the di-lepton system greater than 10 GeV. The two jets must have high transverse momentum greater than 20 GeV and must be well separated in rapidity. The invariant mass of the di-jet system is a powerful tool to select the VBF topology with two energetic jets, so it is necessary to select events with invariant mass of di-jets greater than 500 GeV. The table 3, reviews the acceptance and VBF signal selection criteria. The set of selection criteria was chosen to enhance the signal signature, so in the real data samples, these set of selection cuts can be applied to reduce the background. Once the acceptance cuts are applied, the VBF event selection cuts are imposed to reject the VH contribution and background, the invariant mass of the di-jets can be a good discriminating tools to enhance the VBF signal since in VBF, W boson is decayed leptonically but in VH, the W boson which is produced with the Higgs boson, is decayed hadronically. So in VH mechanism, the jets which are from the decay of W boson, have invariant mass almost equal to W boson mass. So by imposing the cut on Mjj, the contribution of VH can be reduced. As in the real data samples, the dominant background is from top quark and its decay product, so imposing a veto on b-jets is necessary on top of the implemented cuts. More over the central jet veto, (CJV) and the outside lepton veto are needed to suppress all the processes with jets that are produced centrally through QCD and leptons that are outside the rapidity gap between jets. The reason is that VBF is an electroweak process, so jets which are from QCD processes are not expected, moreover the Higgs boson and its decay products, tend to be produced centrally in the rapidity gap between two jets, so all the leptons that are produced outside of the rapidity region should be removed. More details on the background rejection are explained in the reference [6].

The table 4, shows how the VBF signal signature is improving by applying the event selection cuts. It is clear that as the Mjj increases, the VBF signal enhances more. This table also gives the expected number of events for the Higgs production with subsequent decay to W pair which has cross section of 0.0004334 pb for integrated luminosity of 300 fb^{-1} [6].

VBF EVENT SELECTION	
Acceptance cuts	$n_j \geq 2$ $P_j^T \geq 20\ GeV$ $\lvert\eta_j\rvert \leq 4.5$ $M_{jj} \geq 600$
$H \rightarrow WW^* \rightarrow lvlv$ topology	Two opposite charged and opposite flavor leptons, $P_{llep}^T \geq 20\ GeV$, $P_{sublep}^T \geq 10\ GeV$ $\lvert\eta_{lep}\rvert \leq 2.5, \lvert\eta_{sublep}\rvert \leq 2.5$ $M_{ll} \geq 10\ GeV$ $\lvert\Delta\varphi_{ll}\rvert \leq 1.8$ $MET \geq 20\ Ge$

Table 3. Event selection criteria for Higgs production in VBF associated with two tagged jets.

cuts	Total CP-even	Total CP-Odd	VBF CP-odd	VH CP-odd	VBF CP-even	VH CP-even	VBF expected SM Higgs
No cuts	*50000*	*50000*	*21000*	*28500*	*18500*	*31000*	*477.3*
Acceptance without Mjj	*44151*	*45161*	*20322.45*	*24386.94*	*17660*	*26049.09*	*123.14*
Acceptance with Mjj>600 GeV	*7391*	*8341*	*6339.16*	*1918.43*	*5986.7*	*1330.38*	*41.7*
All cuts	*1819*	*2175*	*1957*	*195.7*	*1637.1*	*163.7*	*4.22*

Table 4. Shows the expected number of events for the VBF process.

So far, I have been trying to improve event selection to be able to distinguish a CP-odd coupling from a CP-even Higgs boson coupling in the ggF and VBF channels. In the following sections, the research and the results are presented with details.

Part 2

3.3 CP violation in Higgs production channels

One important question in physics is if the top Yukawa coupling is CP violating or not, i.e. does Higgs boson couple to fermions with both scalar and pseudo-scalar couplings? The ggF Higgs production mechanism is the only mechanism that can probe the CP properties of top Yukawa coupling. On the other hand, its large production cross-section would allow to do such a measurement in run 2 of the LHC.

The VBF production mechanism has a very clean environment, so the signal signature is clear and has a reach kinematical structure and can be distinguished from background, thus this channel can probe the coupling of the Higgs to vector bosons. To search for direct evidence of the nature of CP violating effects in these two production mechanisms at the LHC, we need to define some CP sensitive observables. From the theory chapter we know the tensor structures of the Higgs production in ggF and VBF production mechanisms, have strong correlation in the angle. This angle can provide direct measurement of the CP nature of the Htt Yukawa coupling which is responsible for the effective Hgg vertex and determine the CP properties of the tensor structure of the HWW vertex. So this angle is a good candidate as a CP sensitive observable. To construct this observable, at least two extra energetic jets are needed in the final states to be produced with Higgs. In fact, it can be shown that, in hard scatter processes when jets are very high energetic, the angle dependency of the effective Higgs boson coupling to gluon and the direct coupling of the vector bosons to Higgs can be approximated by the azimuthal angle of these two jets. This azimuthal angle is a powerful tool to search for the CP properties of the tensor structure of these two vertices [1,30,34].

The azimuthal angle of the two tag jets is defined as;

$$\Delta\Phi_{jj} \equiv \Phi_{j1} - \Phi_{j2},\ \Delta\Phi_{jj} \in [0, 2\pi]. \tag{3.1}$$

where Φ_{j1} is defined as the angle of the jet with higher pseudo rapidity. This angle is more sensitive when the two tagged jets are ordered in pseudo-rapidity rather than being ordered by transverse momentum, which means the angle difference between the jet with higher pseudo-rapidity and the second jet with smaller pseudo-rapidity. More details about the comparison between η–ordering and P^T-ordering is given in [34].

In this section, first, the ggF analysis and results are explained, then, the VBF analysis and results are given followed by the comparison of the results of these two channels.

3.3.1 The Higgs boson production through ggF channel with two associated tagged jets

In ggF production channel, the azimuthal angle between two jets, needs to be constructed in a way that it reflects the properties of the Hgg vertex. Figure 9, shows the Feynman diagrams of the scalar and pseudo-scalar Higgs boson couplings to gluons.

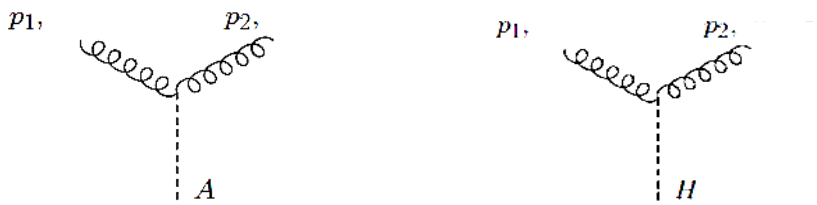

Figure 9. The left diagram shows the pseudo scalar coupling while the right diagram shows the SM model Higgs boson coupling

As it is mentioned in the theory chapter, the Feynman rules derived from the Lagrangian for these vertices are;

for the SM scalar Higgs boson coupling: $-ig_{Hgg}\delta^{a1a2}\ (P_2^{\mu 1}\ P_1^{\mu 2}\ - g^{\mu 1\mu 2}\ P_1 P_2\ )$..

and for the BSM pseudo-scalar Higgs boson coupling: $-ig_{Agg}\delta^{a1a2}\epsilon^{\mu 1\mu 2\rho\sigma}P_{1\rho}P_{2\sigma}$. (3.2)

Where $P_2^{\mu 1}$and $P_1^{\mu 2}$ are the four momenta and P_1 and P_2 are the three momenta of the incoming gluons. It can be seen that these coupling are proportional to the angel between two incoming gluons as;

$$-ig_{Hgg}\delta^{a1a2}\ (P_2^{\mu 1}\ P_1^{\mu 2}\ - g^{\mu 1\mu 2}\ P_1 P_2\ ) \propto\ P_1 P_2\ \cos\psi.$$

$$-ig_{Agg}\delta^{a1a2}\epsilon^{\mu 1\mu 2\rho\sigma}P_{1\rho}P_{2\sigma} \propto\ P_1 P_2 \sin\psi. \quad (3.3)$$

The hard scattering matrix element of the Higgs production with two energetic jets with large rapidity via gluon gluon fusion through top loop can be simplified in the large-m_t limit to

$$|M_{gg\to ggh}|^2 \to \frac{4S^2}{N_C^2-1}\left(\frac{C_A g_s^2}{P_{T1}^2 P_{T2}^2}\right)^2\left(\frac{|C^H(q_{Ta},q_{Tb})|^2}{q_{Ta}^2 q_{Tb}^2}\right). \quad (3.4)$$

Where q_a and q_b are the three momenta of the gluons with C^H and C^A representing the CP- even coupling and the CP- odd coupling to fermions in the loop which they can be approximated by

$$C^H(q_{Ta},q_{Tb}) = \text{-i A}\ |q_{Ta}|\ |q_{Tb}|\cos(\psi_{q1q2}).$$

$$C^A(q_{Ta},q_{Tb}) = \text{i B}\ |q_{Ta}|\ |q_{Tb}|\ \sin(\psi_{q_1q_2}). \quad (3.5)$$

Thus the CP properties of these two couplings are reflected in the angle between the transverse momentums of the two incoming gluons. In a hard scatter process where the tag jets have very high transverse momentum, this angle can be approximated by the azimuthal angle of the two outgoing tag jets that are created by hadronization of the incoming gluons. So the properties of the hard scattering matrix element and the coupling of Higgs boson to two off-shell gluons through the top loop can be studied by this azimuthal angle. [30]

To start this journey, it is important to look at the kinematical distributions of the Higgs boson, two tag jets and the final decay products of the Higgs boson which are leptons. All these distributions are given for both pure CP-odd and pure CP-even couplings for the Higgs mass of 125 GeV at 13 TeV LHC.

First the transverse momentum and the pseudo-rapidity distributions of the Higgs boson are given in figure 10. These plots show the distributions, considering both pure CP-odd and pure CP-even couplings, with all the selection cuts listed in table 1. The plot on the left side in figure 10, shows the normalized distribution of the pseudo rapidity and the plot on the right side shows the normalized distribution of the transverse momentum for both pure CP-even and pure CP-odd couplings.

In order to compare the shape of the distributions, they are normalized in such a way that the area under the curves are the same for both CP-odd and CP-even distributions. It can be seen that the CP-odd and the CP-even case have almost the same shape in both transverse momentum distribution and pseudo-rapidity distribution.

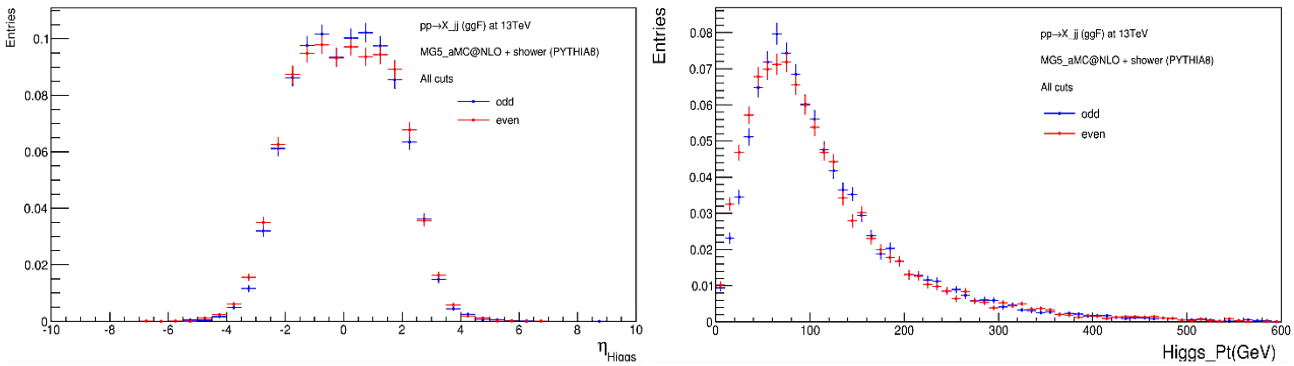

Figure 10 The distribution of the transvers momentum of the Higgs boson for both pure CP-odd distribution in blue and CP-even distribution in red on the right and the pseudo rapidity distribution on the left side.

The given plots in figure 11 and figure 12, show the normalized distributions of the transverse momentum, the angle correlation, pseudo rapidity and invariant mass of the Higgs boson decay products in the final states which are the leptons. The plots show the distributions for both pure CP-odd and pure CP-even couplings after applying all the selection cuts which are listed in table 1. As it is clear from all the plots, there is no significant shape difference between the distribution for the CP-odd and the CP-even Higgs boson coupling to gluons.

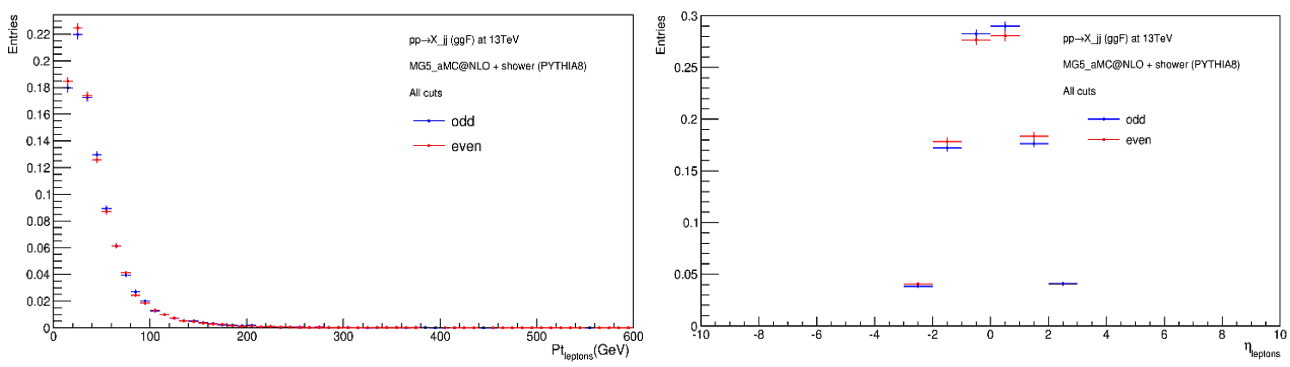

Figure 11. The normalized distribution of the transvers momentum of the leptons on the left and the normalized distribution of the pseudo rapidity of the leptons on the right.

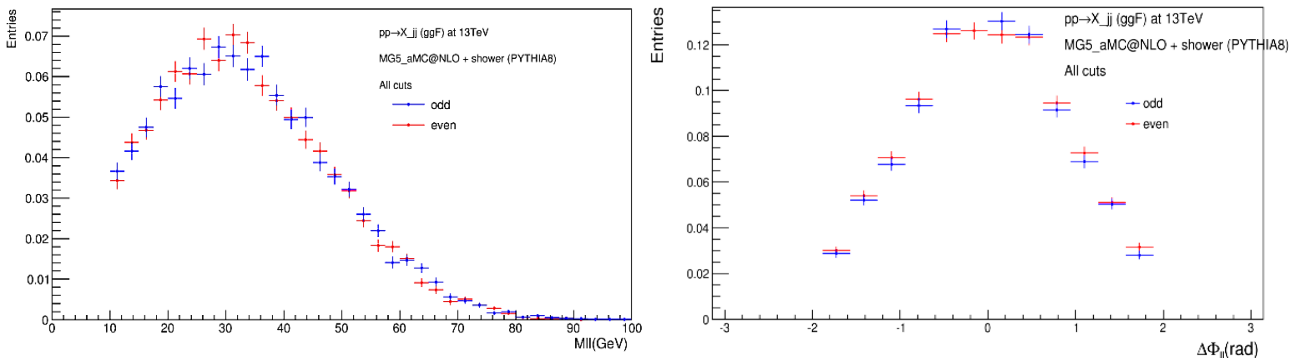

Figure 12. The normalized distribution of the Mll on the left and the normalized distribution of $\Delta\Phi_{ll}$ on the right.

Now if we look at the normalized distribution of the jets transverse momentum which is shown in figure 13 on the right side on top, it can be seen that the distributions for both CP-odd and CP-even couplings, have almost the same shape. The plot indicates that the most of the events are distributed with the transverse momentum higher than 20 GeV, so by applying a selection cut on transverse momentum greater than 20 GeV, we can make sure the jets with high momentum are chosen. The normalized distribution of the pseudo rapidity of the leading jets for both CP-even and CP-odd couplings is shown in the left side and it can be seen that both couplings have almost the same shape. By looking at the plot, it is clear that the jets are more in the forward region as we expected.

The distribution of the invariant mass of the jets with the applied selection cuts is given in figure 14 in the left side and it can be seen that the distribution has the same shape for both CP-even and CP-odd case. In the ggF process, applying the Mjj cuts, suppresses the central jet activity, although it cannot effectively distinguish CP-odd and CP-even states since they have the same distributions [1] and the last plot shows the distribution of the missing transverse energy for both couplings which shows no significant difference between CP-odd and CP-even distributions.

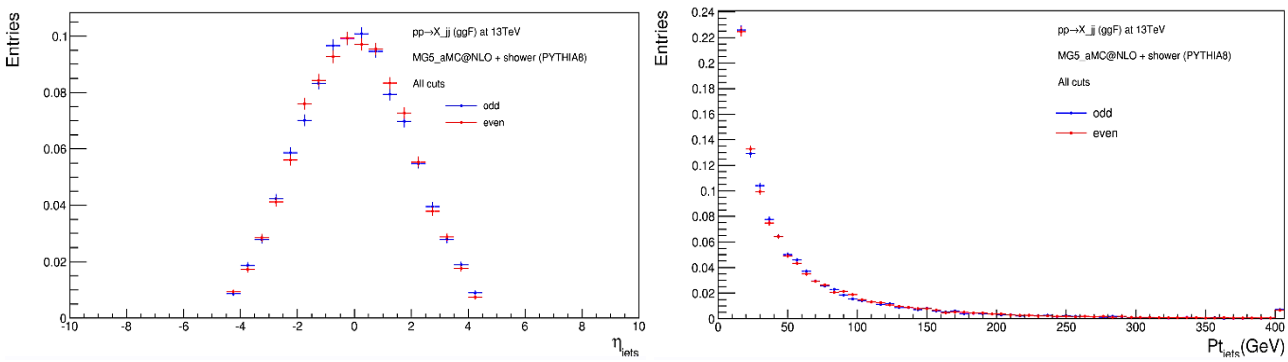

Figure 13. The normalized distribution of the transverse momentum of the jets on the left and the normalized distribution of the pseudo rapidity o the jets on the right.

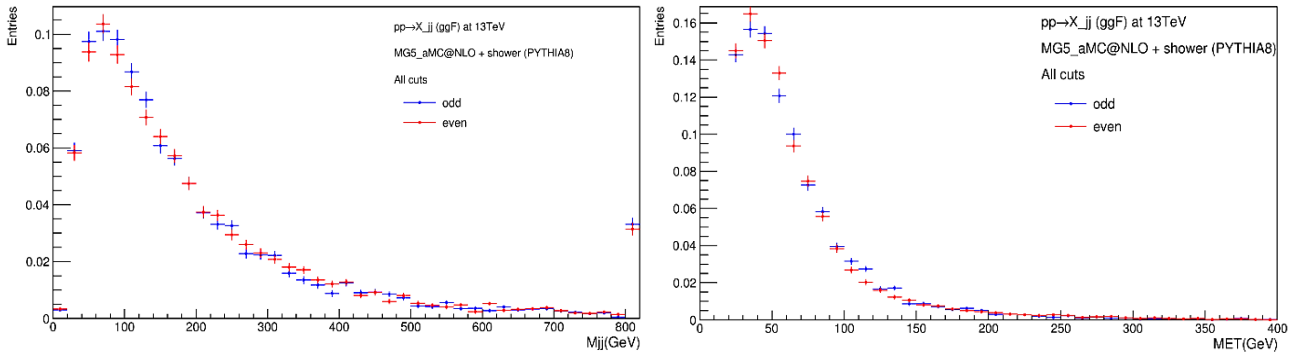

Figure 14. The normalized distribution of the di-jet invariant mass on the left and the normalized distribution of the missing transverse energy on the right.

So far, we have seen the distributions for kinematics of the Higgs boson, jets and leptons. As all the plots indicate, the CP-odd coupling distribution has nearly the same shape as the CP-even distribution, so they are not interesting observables to study the CP-properties of the effective coupling of the Higgs boson to gluons. The next figure shows the expected distributions of the most sensitive observable for the CP nature of the Higgs boson coupling which is the azimuthal angle distribution of the two tagged jets for the purely CP-odd Hgg coupling ($a_2 = k_{Hgg} = 0, a_3 = k_{Agg} = 1$) and the purely CP-even coupling($a_2 = k_{Hgg} = 1, a_3 = k_{Agg} = 0$), for an integrated luminosity of 200fb-1. From theory we expect the distribution of the di-jet correlation, to have different shapes for different CP states of the Higgs boson coupling. Also we expect this difference becomes more significant for higher pseudo rapidity difference between jets. In the plot on the left side, which has all the selection cuts, a slight difference between CP-odd and CP-even distributions is visible. The Plot on the right side, represents the azimuthal angle distribution with an extra cut on pseudo rapidity difference on top of all the applied cuts. By comparing the shape difference evolution in each distribution, it can be seen the pseudo rapidity separation of the two tag jets, is a very powerful cut to enhance the shape difference more efficiently.

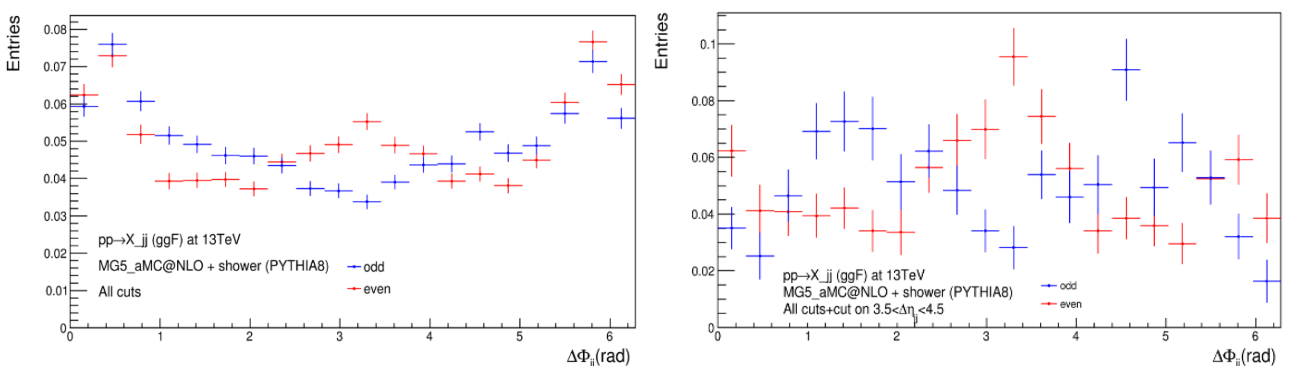

Figure 15. The plots for $\Delta\Phi jj$ distribution. The first plot on left is the normalized distribution with all the cuts, the plot on the right is the normalized distribution with an extra cut on 3.5<|$\Delta\eta jj$ |<4.5.

Fitting and interpreting the ΔΦjj distribution

As we know, $\Delta\Phi_{jj}$ is a parity odd observable, therefor, parity violation appears as an asymmetry in the $\Delta\Phi_{jj}$ distribution for the process pp → Hjj . Since the QCD couplings are all parity conserving, so the parity violations must come from a parity odd Higgs coupling. If we look at the effective Hgg vertex and the tensor structure in equation 3.47 in the theory chapter, we see the parity violation can only come from a_3 in the effective Hgg vertex which is a parity odd coupling. In the real data, if CP-odd coupling exists, it occurs at the same time with the SM CP-even coupling, i.e. the coupling might be a mixture of CP-odd and CP-even states which depends on the complex mixing angle of each coupling, thus, observation of any asymmetry in the $\Delta\Phi_{jj}$ distribution would directly demonstrate the CP violation in Higgs sector which has originated from a_3 [37].

Since the azimuthal angle difference of the two tagged jets, $\Delta\Phi_{jj}$, and the pseudo rapidity difference between two tagged jets, $\Delta\eta_{jj}$, are sensitive to the CP nature of the Higgs boson couplings, to study the CP-odd coupling, it is important to use the projection of the $\Delta\Phi_{jj}$ distribution in different pseudo-rapidity intervals and then fit the distributions to extract information. The fit function is become more informative and efficient when it comes from the couplings and can reflect the properties of the tensor structure and matrix element. A good option would be fitting a function which has the $\Delta\Phi_{jj}$ dependence, since it can describe the couplings and the matrix element. As we have seen in section 3.3.1, the couplings of the Hgg and Agg vertices are proportional to azimuthal angle as;

for CP-odd coupling $\quad -ig_{Agg}\delta^{a1a2}\epsilon^{\mu1\mu2\rho\sigma}P_{1\rho}P_{2\sigma} \propto 2P_{1\sigma}\,P_{2\sigma}\ \sin\Delta\Phi\,jj.$

and for CP-even coupling $\quad -ig_{Hgg}\delta^{a1a2}\ \left(P_2^{\mu1}\ P_1^{\mu2}\ - g^{\mu1\mu2}\,P_1P_2\ \right) \propto const +\ P_1P_2\cos\Delta\Phi\,jj.$

Considering the fact that the production cross-section is proportional to the matrix element squared and the square of the couplings, to find a function which can reflect the production cross section and the matrix element properties, the square of the sum of the couplings should be calculated and the fit function becomes;

$$F(\Delta\Phi jj) \propto (const +\ P_1P_2\cos\Delta\Phi\,jj\quad +\ 2P_{1\sigma}\,P_{2\sigma}\ \sin\Delta\Phi\,jj)^2 \cong\ const + a\cos\Delta\Phi jj + b\cos 2\Delta\Phi jj +\ c\sin\Delta\Phi jj.$$

And by adding higher order gluons contributions, the function can be approximated by;

$$F(\Delta\Phi jj) =\ C0\ [\ 1 + C1\times\cos\Delta\Phi jj + C2\times\cos 2\Delta\Phi jj + C3\times\sin\Delta\Phi jj + C4\times\sin 2\Delta\Phi jj + C5\times \cos 3\Delta\Phi jj + C6\times\cos 4\Delta\Phi jj + C7\times\cos 5\Delta\Phi jj] \tag{3.6}$$

Where the term " $\cos\Delta\Phi_{jj}$ " has a contribution only from CP-even coupling, the term " $\sin\Delta\Phi_{jj}$", has a contribution only from CP-odd coupling and the rest of the terms represent the mixing between CP-odd and CP-even couplings which depend on their complex mixing phases.

The function in Eq.4.6 is used to fit the projection of the ΔΦjj distribute on different jet pseudo-rapidity separation intervals which is obtained from the 2-D histogram of $\Delta\Phi_{jj}$ vs $\Delta\eta_{jj}$. The results are given in the following plots.

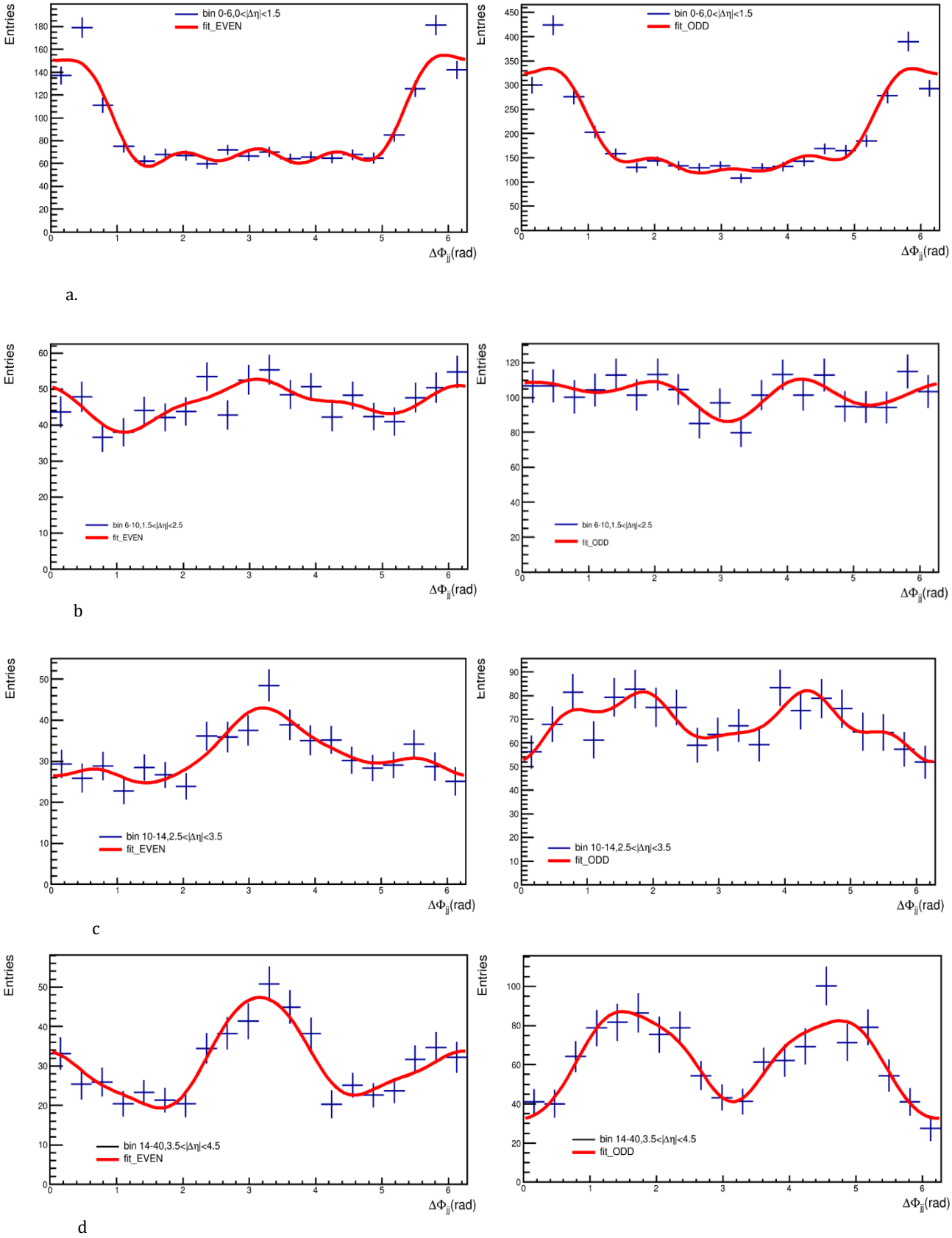

Figure 16: The plots on the left side show the distribution of the ΔΦjj for CP-even and the plots on the right show the distribution of the ΔΦjj for the CP-odd couplings. All plots show the projection of ΔΦjj, on pseudo rapidity intervals a) 0<| Δη|<1.5, b) 1.5<| Δη|<2.5, c) 2.5<| Δη|<3.5, d) 3.5<| Δη|<4.5.

The first plot on the left is the distribution for CP-even coupling and the plot on the right is the distribution for CP-odd coupling. Both show the $\Delta\Phi_{jj}$ distribution for 0< | Δηjj |<1.5. By comparing these two plots, it can be seen for lower values of pseudo rapidity difference between the two jets, the CP-odd and the CP-even distributions have almost the same shape and the same characteristics.

When the pseudo rapidity difference increases, as we can see from the figure 16. b, for 1.5 ≤|Δηjj|≤ 2.5, the CP-odd and the CP-even distribution start to become more distinct, for the CP-odd distribution, a minimum is found around π , while in the distribution for CP-even, a maximum around π can be observed.

The next set of plots in figure 16. c, show the $\Delta\Phi_{jj}$ distribution for 2.5 ≤|Δηjj|≤ 3.5. In the left plot which shows the distribution in case of the pure CP-even coupling, it can be seen two maxima and the minimum, have become more pronounced by increasing Δηjj. Moreover, the difference between the CP-odd coupling and the CP-even coupling is more noticeable.

The plots in figure16. d, represent the distributions for 3.5 ≤|Δηjj| ≤ 4.5. The $\Delta\Phi_{jj}$ distribution, in case of CP-odd coupling, has a minimum in π where the distribution in case of CP-even has a maximum. So the difference between these two distributions has become maximized.

Now if we look at the table.5, which shows the coefficients of the fitted function, we see for all the plots, the coefficients "C1", which is associated with the term "$\cos(x)$", and "C2", which is associated with the term "$\cos(2x)$ ", have the biggest values and they increase in each plot by increasing the pseudo rapidity difference. Moreover it can be seen that the value of C2 for CP-odd coupling is very different from the corresponding value for CP-even coupling and the difference has become maximized by increasing the pseudo rapidity difference between jets.

The coefficient C3 has a very small value which means contribution of the "$\sin(x)$" term is very small. In fact due to different complex mixing phases, we don't see the effect of "$\sin(x)$" term because some fraction of it, is absorbed in "$\cos(2x)$" and in other modulations. In addition, the rest of the coefficients are almost zero within the error. One should keep in mind that the contribution from the CP-odd and CP-even depends on the complex mixing phase.

As a matter of fact, CP-violation arises from C2, because this coefficient has the biggest differences between CP-odd and CP-even so the effect of CP violation is visible although "$\sin(x)$" term is small.

In conclusion, based on expectation from theory, as the jets become more forward, the distribution of their azimuthal angle becomes more distinct for CP-odd and CP-even states which means if the CP-odd Higgs boson coupling exists, we should be able to see its effect when the jets have a large rapidity difference.

Figure 17, shows the angular distribution for simulated signal samples of CP-mixed states that are generated with the same percent for both CP-odd and CP-even is represented for different pseudo rapidity intervals. From the plots, it can be seen that there is a slight difference between CP-mix distribution and pure CP-odd/CP-even distributions. Moreover, we see as the pseudo rapidity difference increases, the

distribution for CP-mixed state becomes more asymmetric. In fact, the coefficient C4, which corresponds to "$\sin(2x)$" term, is big for the distribution which indicates the mixing between CP-odd and CP-even coupling. Indeed the superposition of CP-odd and CP-even states depend on their complex mixing angle which is a free parameter, so the contribution from CP-odd can be distinguished with a mixing phase term from the SM CP- even Higgs boson.

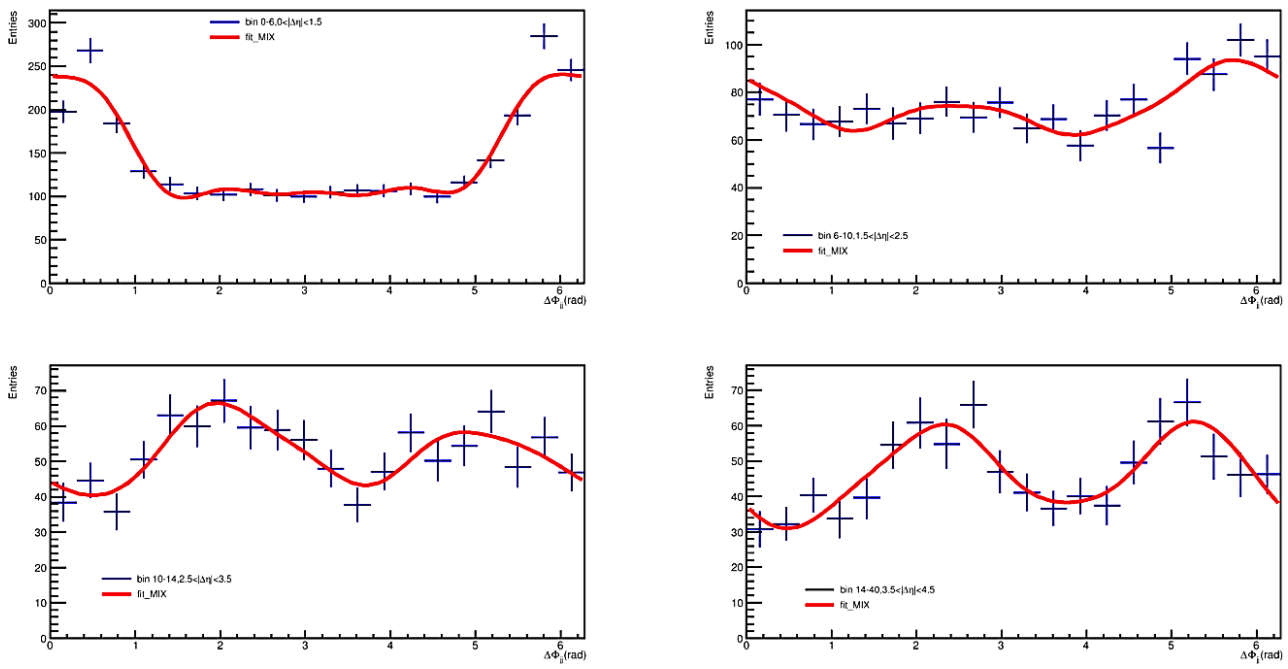

Figure 17, The projection of the azimuthal angle distribution on different pseudo rapidity intervals for CP-mix coupling. The first plot on top left represents the distribution for 0<| Δη|.<1.5, the top right shows the distribution for 1.5<| Δη|.<2.5, the plot on bottom left for 2.5<| Δη|.<3.5 and the last plot on bottom right shows the distribution for 3.5<| Δη|.<4.5.

Coefficients	| Δηjj |	CP-odd	CP-even	CP-mix
C0	0<| Δηjj|<1.5	198.97±2.95	90.41±1.31	144.46±2.12
	1.5<| Δηjj |<2.5	101.99±2.02	46.30±0.90	74.3±1.46
	2.5<| Δηjj |<3.5	68.81±1.70	31.38±0.77	52.23±1.24
	3.5<| Δηjj |<4.5	62.49±1.85	30.36±0.83	46.80±1.34
C1	0<| Δηjj|<1.5	0.53±0.02	0.45±0.02	0.45±0.02
	1.5<| Δηjj |<2.5	-0.038±0.027	-0.04±0.02	0.11±0.02
	2.5<| Δηjj |<3.5	-0.053±0.033	-0.18±0.03	-0.06±0.03
	3.5<| Δηjj |<4.5	-0.098±0.03	-0.18±0.04	-0.06±|0.03
C2	0<| Δηjj|<1.5	0.21±0.02	0.28±0.019	0.24±0.01
	1.5<| Δηjj |<2.5	-0.035±0.028	0.091±0.02	0.05±0.02
	2.5<| Δηjj |<3.5	-0.132±0.034	0.115±0.034	-0.11±0.033
	3.5<| Δηjj |<4.5	-0.38±0.04	0.31±0.038	-0.099±0.03
C3	0<| Δηjj|<1.5	0.0097±0.018	-0.024±0.018	-0.02±0.01
	1.5<| Δηjj |<2.5	0.0159±0.028	-0.03±0.027	-0.044±0.02
	2.5<| Δηjj |<3.5	0.027±0.034	-0.08±0.033	0.03±0.03
	3.5<| Δηjj |<4.5	0.036±0.045	-0.057± 0.035	-0.029±0.04
C4	0<| Δηjj|<1.5	0.0068±0.019	-0.027±0.019	-0.01±0.01
	1.5<| Δηjj |<2.5	0.027±0.028	-0.030±0.027	-0.11±0.02
	2.5<| Δηjj |<3.5	0.047±0.035	0.011±0.034	-0.14±0.033
	3.5<| Δηjj |<4.5	0.010±0.041	0.012±0.038	-0.25±0.039
C5	0<| Δηjj|<1.5	0.041±0.022	0.065±0.019	0.05±0.02
	1.5<| Δηjj |<2.5	0.068±0.028	-0.033±0.027	0.005±0.02
	2.5<| Δηjj |<3.5	0.023±0.035	-0.056±0.034	0.01±0.033
	3.5<| Δηjj |<4.5	-0.0034±0.041	-0.067±0.036	-0.02±0.04
C6	0<| Δηjj|<1.5	-0.072±0.022	-0.044±0.016	-0,05±0.02
	1.5<| Δηjj |<2.5	-0.011±0.028	0.025±0.028	-0.004±0.02
	2.5<| Δηjj |<3.5	-0.023±0.035	0.0089±0.035	0.022±0.033
	3.5<| Δηjj |<4.5	-0.028±0.041	-0.017±0.035	-0.023±0.039
C7	0<| Δηjj|<1.5	-0.079±0.013	-0.092±0.019	-0.05±0.01
	1.5<| Δηjj |<2.5	0.0002±0.028	-0.009±0.028	-0.01±0.02
	2.5<| Δηjj |<3.5	-0.051±0.035	-0.021±0.034	-0.01±0.033
	3.5<| Δηjj |<4.5	0.034±0.041	0.028±0.035	0.011±0.039

Table 5, The coefficients of the fitted function for ggF production channel for pure CP-even and pure CP-odd couplings.each coeffiient is given for different pseudo rapidity intervals.

3.3.2 The Higgs boson production through VBF channel

In an attempt to study the CP properties of the tensor structure of the HWW vertex, an observable needs to be defined based on the tensor structure properties. Previously, it was shown for ggF process, the azimuthal angle between the two jets is a promising CP-sensitive observable. Accordingly, this angle is considered as an observable for VBF studies as well.

The Feynman diagram of the HVV vertex is shown in figure 18.

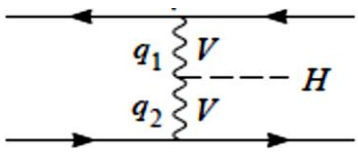

Figure 18, The Feynman diagram of the Higgs production through VBF channel,where q_1 and q_2 represent the momenta of the incoming vector bosons.

The most general form of the tensor structure of this vertex is given in equation 2.49 where a_3 and a_2 are momentum dependent form factors [37,38].

Some jet kinematics like di-jet invariant mass or transvers momentum, depend on the form factors [38] so without specifying a physical model it is impractical to use the distribution of them to study the CP properties of the vertex. But the azimuthal angle between two jets is insensitive to the form factors so the shape of $\frac{d\sigma}{d\Delta\Phi_{jj}}$ can provide information on the CP properties and make distinction between them.

The given tensor structure, shows the coupling of a spin-zero Higgs boson to two gauge bosons. If we work in high energy limits with two high energetic jets, it can be assumed the transverse momentum of the vector bosons are transferred to the jets , then the tensor structure can be simplified as ;

$$T^{\mu\nu}(q_1, q_2) \propto \quad const + a_2(p_{1jet}, p_{2jet})\, P^T_{1jet}.P^T_{2jet} \quad + \; a_3(p_{1jet}, p_{2jet})\varepsilon^{\mu\nu\rho\sigma} P^T_{1jet} P^T_{2jet}.$$

which a_2 and a_3 represent the CP-odd and the CP-even coupling respectively, P^T_{1jet} and P^T_{2jet} represent the four momenta of the two tagged jets and p_{1jet} and p_{2jet} represent their three momenta. Both terms depend on the azimuthal angle between two tag jets, so each term can be parametrized in terms of angle as

$$\text{CP-odd term} \quad \propto \quad a_3(p_{1jet}, p_{2jet}) p^T_{1jet} p^T_{2jet}\, sin\, \Delta\Phi_{jj}.$$

$$\text{CP-even term} \quad \propto a_2(p_{1jet}, p_{2jet})\, p^T_{1jet} p^T_{2jet} \cos \Delta\Phi_{jj}.$$

As a result, the information about the CP nature of the HVV vertex can be extracted from this angle. Similar to the scenario for the ggF process in section 3.3.1, a function which can describe the properties of the matrix element and reflect the production cross section will be fitted to the distribution of the $\Delta\Phi_{jj}$.

The same function in Eq.3.6 which is used for ggF, can efficiently describe the distribution and extract the information. To start the VBF analysis, first the distribution of the transverse momentum and the

pseudo rapidity of the Higgs boson for pure CP-even and pure CP-odd couplings are given in figure 19 for M_h=125 GeV in the center of mass energy of 13 TeV with the integrated luminosity of 300 fb-1.

The plot on the left side shows the normalized distribution of the transverse momentum of the Higgs boson and the plot on the right side shows the normalized distribution of the pseudo rapidity of the Higgs boson. Both plots represent the distributions for both pure CP-odd and pure CP-even coupling with all the selection cuts that are listed in table 3. As it can be seen from the plots, the shapes for both CP-even and CP-odd are almost the same. One cannot say about the rate difference due to rate dependency on the production cross-section which can be calculated from different models in BSM. As it is expected for the VBF signal, in most of the events, the Higgs boson tends to be produced centrally.

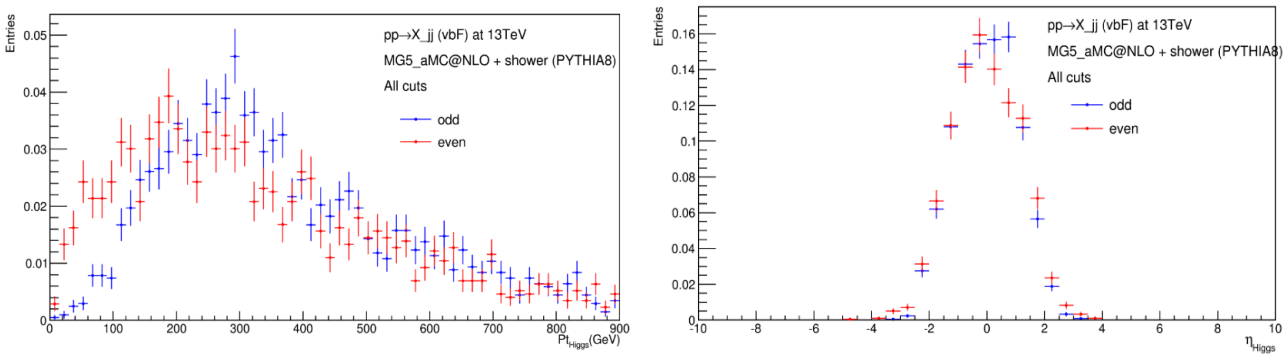

Figure 19.The plot on the left side shows the normalized distribution of the transverse momentum of the Higgs boson and the plot on the right side shows the pseudo rapidity of the Higgs boson. Both plots show the distributions for pure CP-odd coupling in blue and pure CP-even coupling in red.

If we also look at the distribution of the kinematics of the Higgs boson decay products, it is visible as it is expected for VBF signal topology, the leptons are produced centrally, two energetic jets that are highly seperated in rapidity, force the decay products to become more central [6,36]. The plot on the left side of the figure 20, show the normalized distribution of the transverse momentum of the leptons and the plot on the right side is the normalized distribution of the pseudo rapidity of the leptons. Both plots present distributions for both CP-even and CP-odd couplings with all the applied cuts in table.3.It can be seen that both distributions have the same shape for both couplings.

Figure 21, shows the normalized distribution of the di-lepton correlation on the left and the invarinat mass of the leptons on the right with all the applied cuts. In both plots, there is no significant difference between CP-odd and CP-even coupling distributions.

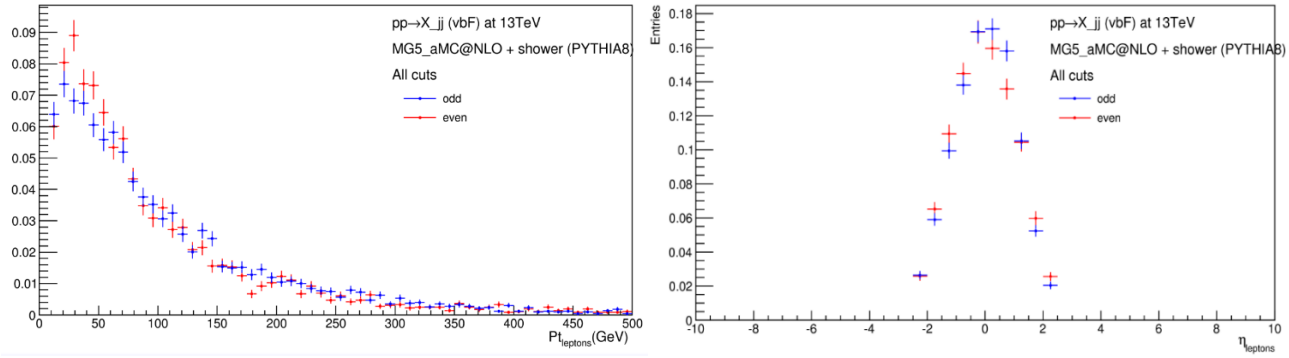

Figure 20, The normalized distribution of the transverse momentum of leptons on the lef and the normalized distribution of the pseudo rapidiy of leptons on the right.

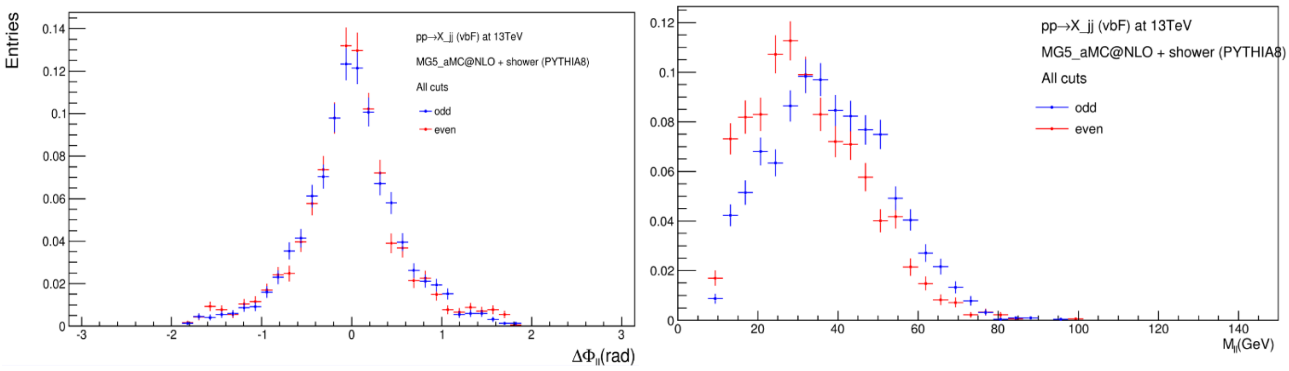

Figure 21, The normalized distribtuon of the di-lepton correlation on the left and the normalize distribution of thr di-lepton invariant mass on the right.

The next set of plots are the distribuitions of the jets kinematics. The first plot in figure 22, is the distribution of the transverse momentum of the two tag jets, with all the applied cuts, for the CP-odd and the CP-even case, it can be seen they have almost the same distribution shape. The plot on the right side is the normalized distribution of the pseudo rapidity of the jets with all the applied cuts. As it is expected for the VBF topology, in most of the events, jets are more in the forward region. The last plot shows the normalized distribution of the di-jet invariant mass with all the cuts except cut on Mjj. There is no shape difference between the CP-odd distribution and the CP-even distribution for all the given plots.

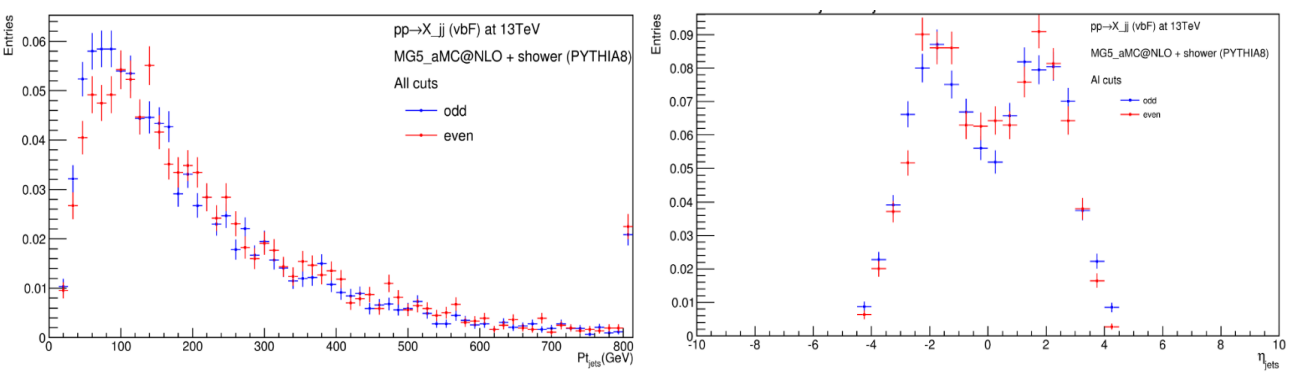

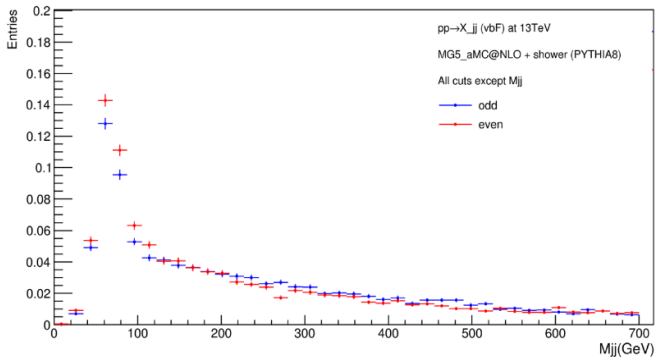

Figure 22, The normalized distribution of the transverse momentum of the jets on top left, the normalized distribution of the pseudo rapidity of the jets on top right and the normalized distribution of the di-jets invariatn mass.on the middle.

Fitting and interpreting the $\Delta\Phi_{jj}$ distribution

In all the plots that are presented so far, there is no significant difference between the CP-even and the CP-odd distributions. Moreover without knowing the parameters for the Lagrangian beyond the Standard Model, it is not possible to compare the rate difference.

As we have seen in the theory chapter, all these kinematical distributions that are given so far, depend on the form factors and form factors depend on the physical model. The only variable that is form factor independent and is CP sensitive at the same time, is the azimuthal angle between the two tag jets. The next set of plots show the distribution of this angle for pure CP-even and pure CP-odd coupling in the HWW vertex for the Higgs mass of 125 GeV, at the center of mass energy of 13 TeV at the LHC.

The distribution in figure 23 on the left side, has all the selection cuts that are listed in table.3, from the plot, we can see the shape difference between the CP-odd and the CP-even coupling is already visible. By adding a selection cut on the rapidity difference of the two tag jets, the difference between the CP-odd and CP-even increases noticeably which is presented in the plot on the right side, So, as it is expected based on theory, the pseudo rapidity separation of the two tag jets and the di-jet invariant mass, are very powerful selections to enhance the shape difference. So we expect as rapidity separation increases, the analyzing power of the azimuthal angle to see the shape difference increases more. More details about the theoretical discussions are given in [36-38].

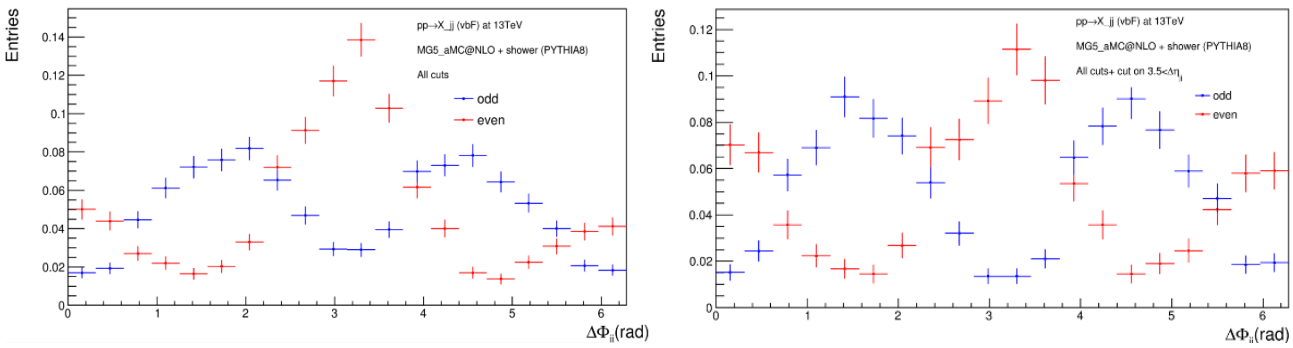

Figure 23, the plot on the left side show th distribution of $\Delta\Phi jj$ with all the cuts and the plot on the right side show the distribution of $\Delta\Phi jj$ with extra cut on $3\leq|\Delta\eta jj|$.

Considering the fact that di-jet correlation carries information about the CP properties of the HVV vertex and pseudo rapidity separation increases its power, an efficient way to study $\Delta\Phi_{jj}$ as we have seen for ggF analysis, is projecting the $\Delta\Phi_{jj}$ distribution onto the pseudo rapidity difference intervals. The results are represented in figure 24.

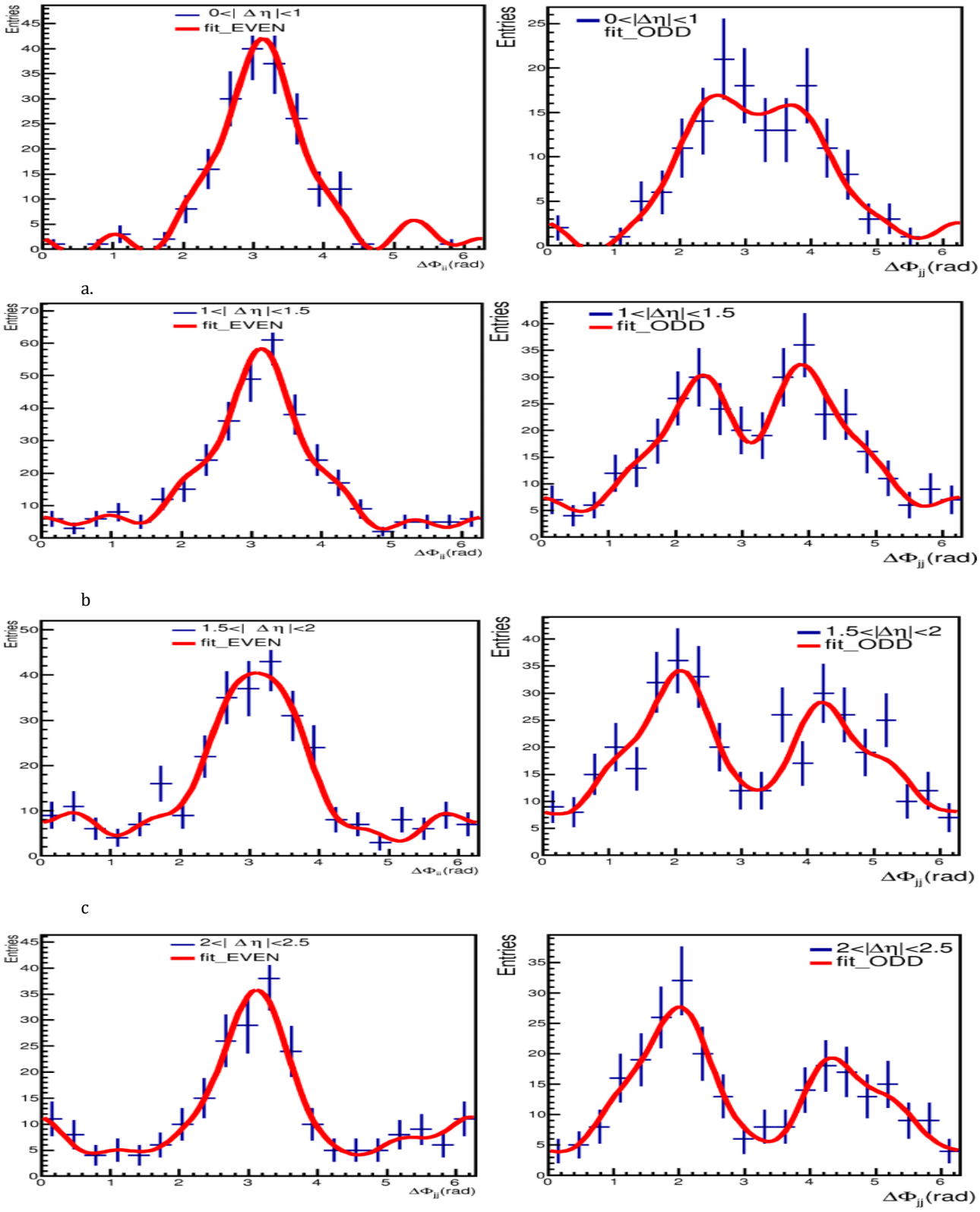

a.

b

c

d

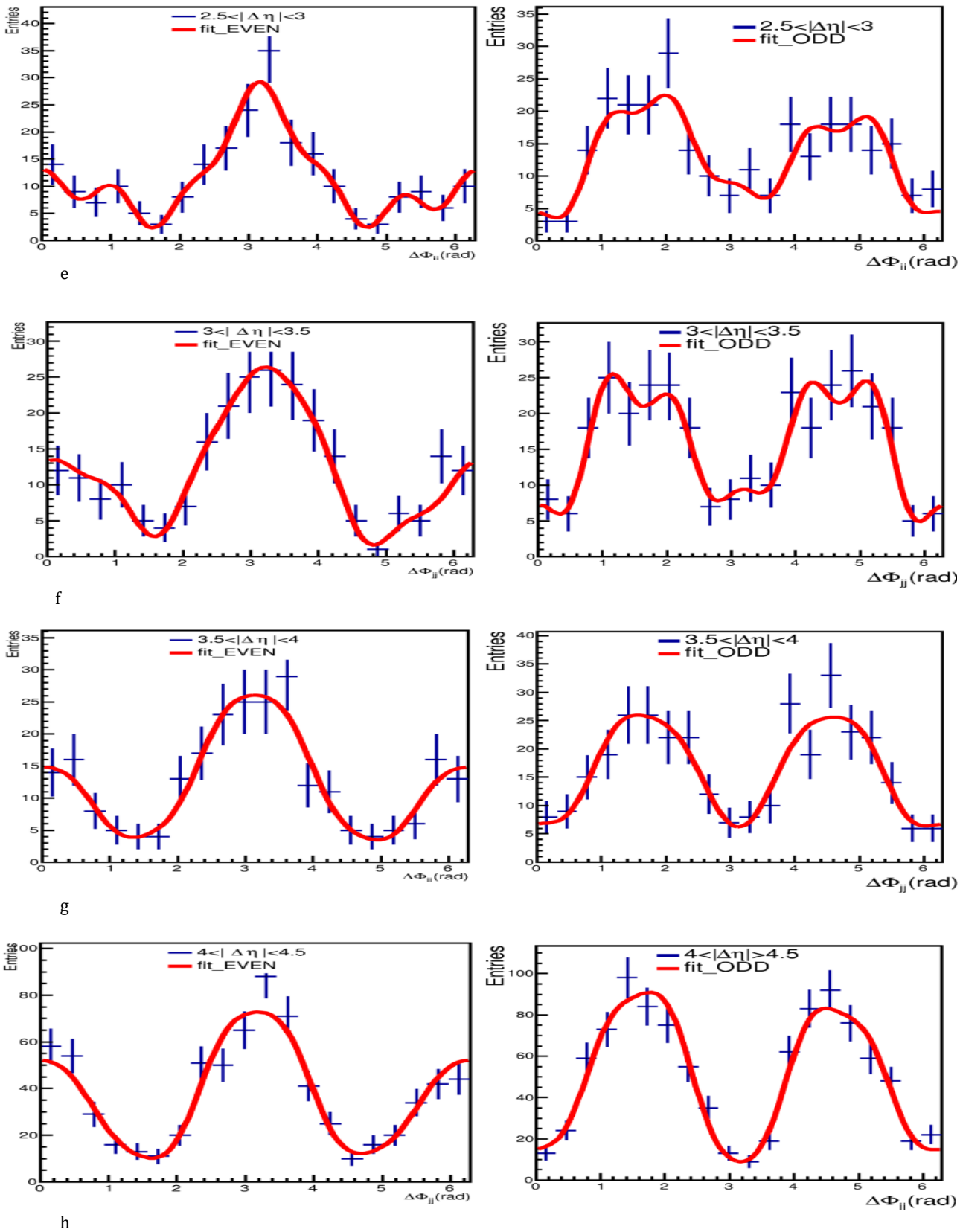

Figure 24, The projection of the azimuthal angle distribution on different pseudo rapidity intervals for pure CP-even coupling on the left and pure CP-odd on the right. The figures in a) present the distribution for 0≤|Δηjj|≤ 1, figures in b) present for 1≤|Δηjj|≤ 1.5, figures in c) present for 1.5≤|Δηjj|≤ 2, figures in d) show for 2≤|Δηjj|≤ 2.5, figures in e) shows for 2.5≤|Δηjj|≤ 3 , figures in f) show for 3≤|Δηjj|≤ 3.5, figures in g) present the distribution for 3.5≤|Δηjj|≤ 4 and the last plots in h) represent the distributions for 4≤|Δηjj|≤ 4.5

The plots on the left, represent the distributions of the azimuthal angle for purely CP-even coupling and the plots on the right, represent the distributions for the purely CP-odd coupling for different pseudo rapidity difference between two jets. The plots in figure 20.a represent the distributions for $0 \leq |\Delta\eta jj| \leq 1$. In contradiction to the ggF channel, the distribution for CP-even in low pseudo rapidity ranges is already different from the distribution for CP-odd, since the invariant mass of the jets, is an important quantity to discriminate a CP-odd coupling from a CP-even coupling in VBF production channel. As it is clear from the plots, by increasing the $\Delta\eta jj$, the difference between CP-odd and CP-even distributions become more distinct. In the last set of plots in figure 20.h, the distributions for $4 \leq |\Delta\eta jj| < 4.5$ are represented and it is obvious that the difference between CP-odd distribution and CP-even distribution has become maximized. The CP-even has a sharp maximum at π while the CP-odd has a minimum at π and two local maximums around $\Delta\Phi_{jj} \sim 2$ and $4 < \Delta\Phi_{jj} < 5$.

If we compare the coefficients of the fitted function which are listed in table 6, in general, we could say the coefficients C1, C2 and C5 are non-zero, while the rest of the coefficients are negligible within the errors. The coefficient C1 is bigger for CP-even distribution than CP-odd distribution and it decreases as the pseudo rapidity difference increases. The coefficient C2 which corresponds to the "$\cos(2x)$" term, increases as the pseudo rapidity difference increase and it has completely different values for CP-odd and CP-even case. The main part of the CP-violation is from this term because it represents the maximum difference between CP-odd and CP-even couplings as we have seen for the ggF channel. Moreover, it can be seen that the coefficient C5 which corresponds to "$\cos(3x)$" term, which is from the mixing, has different non vanishing values for CP-odd and CP-even case. With the same scenario as we had for ggF samples, the mixing between CP-odd and CP-even states depends on their complex mixing phase. In fact this phase is the reason that we can have different modulations in addition to "$\cos(x)$" and "$\sin(x)$" terms.

To sum up, as we expected, the pseudo rapidity difference between two jets and their invariant mass are the powerful quantities for discrimination of CP-odd and CP-even states. As the pseudo rapidity difference increases, the analyzing power of the azimuthal angle increases and the distinction between these two states becomes maximized. Further, the reason that some coefficients like C3 are small and we don't see the effect of "$\sin(x)$" or "$\sin(2x)$" terms, is that the contribution from each coupling depends on its complex mixing angle and it determines which term of the function can have bigger contribution in the angular distribution.

Coefficient	| Δηjj |	VBF-odd	VBF even
C0	0<| Δηjj|<1	7.33±0.67	9.89±0.82
	1<| Δηjj|<1.5	16.79±0.92	16.57±0.91
	1.5<| Δηjj|<2	18.47±0.96	14.58±0.85
	2<| Δηjj|<2.5	12.98±0.80	11.72±0.76
	2.5<| Δηjj|<3	12.99±0.80	11.28±0.75
	3<| Δηjj|<3.5	15.65±0.88	11.91±0.77
	3.5<| Δηjj|<4	16.34±0.90	12.38±0.78
	4<| Δηjj|<4.5	50.10±1.58	37.13±1.45
C1	0<| Δηjj|<1	-1.14±0.14	-1.45±0.11
	1<| Δηjj|<1.5	-0.67±0.06	-1.16±0.06
	1.5<| Δηjj|<2	-0.32±0.06	-0.90±0.07
	2<| Δηjj|<2.5	-0.26±0.07	-0.73±0.09
	2.5<| Δηjj|<3	-0.14±0.07	-0.53±0.10
	3<| Δηjj|<3.5	-0.07±0.06	-0.54±0.09
	3.5<| Δηjj|<4	-0.12±0.06	-0.46±0.1
	4<| Δηjj|<4.5	-0.03±0.03	-0.24±0.06
C2	0<| Δηjj|<1	0.24±0.11	0.90±0.12
	1<| Δηjj|<1.5	-0.11±0.07	0.67±0.07
	1.5<| Δηjj|<2	-0.40±0.06	0.68±0.07
	2<| Δηjj|<2.5	-0.58±0.07	0.73±0.08
	2.5<| Δηjj|<3	-0.59±0.07	0.62±0.08
	3<| Δηjj|<3.5	-0.59±0.07	0.66±0.079
	3.5<| Δηjj|<4	-0.61±0.07	0.69±0.07
	4<| Δηjj|<4.5	-0.78±0.03	0.72±0.05
C3	0<| Δηjj|<1	-0.01±0.10	-0.02±0.08
	1<| Δηjj|<1.5	-0.07±0.09	0.05±0.05
	1.5<| Δηjj|<2	0.09±0.07	0.08±0.06
	2<| Δηjj|<2.5	0.21±0.09	0.02±0.06
	2.5<| Δηjj|<3	0.11±0.09	-0.001±0.06
	3<| Δηjj|<3.5	0.009±0.08	0.03±0.06
	3.5<| Δηjj|<4	0.014±0.08	0.014±0.06
	4<| Δηjj|<4.5	0.081±0.04	-0.02±0.04
C4	0<| Δηjj|<1	-0.09±0.14	-0.13±0.09
	1<| Δηjj|<1.5	0.010±0.09	0.0004±0.06
	1.5<| Δηjj|<2	0.09±0.07	-0.03±0.07
	2<| Δηjj|<2.5	-0.17±0.08	-0.14±0.07
	2.5<| Δηjj|<3	-0.11±0.08	0.08±0.08
	3<| Δηjj|<3.5	0.05±0.07	0.17±0.08
	3.5<| Δηjj|<4	0.03±0.07	0.004±0.08
	4<| Δηjj|<4.5	0.006±0.03	0.017±0.05

C5	0<| Δηjj|<1	0.20±0.11	-0.48±0.11
	1<| Δηjj|<1.5	0.23±0.07	-0.27±0.07
	1.5<| Δηjj|<2	0.21±0.07	-0.20±0.07
	2<| Δηjj|<2.5	0.22±0.08	-0.29±0.09
	2.5<| Δηjj|<3	0.02±0.09	-0.20±0.09
	3<| Δηjj|<3.5	0.04±0.08	-0.03±0.09
	3.5<| Δηjj|<4	0.08±0.07	-0.004±0.08
	4<| Δηjj|<4.5	0.08±0.04	-0.05±0.06
C6	0<| Δηjj|<1	-0.06±0.12	0.10±0.09
	1<| Δηjj|<1.5	-0.11±0.09	0.13±0.07
	1.5<| Δηjj|<2	-0.10±0.07	0.05±0.08
	2<| Δηjj|<2.5	-0.06±0.08	0.20±0.08
	2.5<| Δηjj|<3	-0.03±0.08	0.04±0.09
	3<| Δηjj|<3.5	-0.05±0.08	-0.06±0.08
	3.5<| Δηjj|<4	-0.01±0.08	-0.002±0.08
	4<| Δηjj|<4.5	-0.02±0.04	-0.007±0.06
C7	0<| Δηjj|<1	0.108±0.12	-0.07±0.11
	1<| Δηjj|<1.5	0.13±0.11	-0.13±0.07
	1.5<| Δηjj|<2	-0.009±0.07	-0.01±0.07
	2<| Δηjj|<2.5	-0.045±0.08	-0.02±0.08
	2.5<| Δηjj|<3	0.012±0.080	0.01±0.08
	3<| Δηjj|<3.5	0.042±0.07	0.03±0.08
	3.5<| Δηjj|<4	0.063±0.07	0.01±0.08
	4<| Δηjj|<4.5	0.006±0.03	0.03±0.05
C8	0<| Δηjj|<1	0.011±0.13	0.21±0.12
	1<| Δηjj|<1.5	-0.020±0.11	0.15±0.05
	1.5<| Δηjj|<2	0.059±0.07	-0.09±0.07
	2<| Δηjj|<2.5	0.060±0.08	0.076±0.08
	2.5<| Δηjj|<3	0.138±0.07	0.20±0.08
	3<| Δηjj|<3.5	0.180±0.07	0.06±0.08
	3.5<| Δηjj|<4	0.022±0.07	-0.03±0.08
	4<| Δηjj|<4.5	0.056±0.03	-0.03±0.05

Table 6,The coeeficients of the fitted function for VBF production channel for pure CP-even and pure CP-odd couplings.each coeffiient is given for different pseudo rapidity intervals.

4 CONCLUSION AND OUTLOOK

In this thesis, I studied the CP-nature of the Higgs boson coupling in ggF and VBF production channels with the help of CP-sensitive variables and compared them with expectations from theory in both channels.

In this analysis, we have seen that for Higgs production in association with two high energetic jets in both channels, the selections cuts are applied to enhance the signal signature and the azimuthal angle of the two jets is considered as a CP sensitive variable which carries information of the Higgs boson couplings.

In the results, it was shown that in ggF process, as it is expected from theory, the pseudo rapidity difference can decode the information in the azimuthal angle distribution and by increasing it, different distributions become appear for CP-odd and CP-even couplings. Moreover it was shown that the fit function in Eq.3.6 can describe the distribution of the azimuthal angle for different CP states in different pseudo rapidity ranges.

In VBF channel, it was shown that by selecting the jets with high invariant mass, the azimuthal angle distribution becomes different for CP-even and CP-odd states and by increasing the pseudo rapidity gap between two jets, the difference between the distributions becomes maximized. So in this channel, invariant mass and pseudo rapidity difference, increase and maximize the analyzing power of the angular distribution.

In conclusion, in reality, if the CP-odd coupling exists, we can see its effect when jets are highly separated in rapidity. The Higgs boson can be a CP-odd, CP-even or a mixed state, which depends on the complex mixing phases of each state which are free parameters and were not studied in this thesis. One could fit a function for different mixing phases to measure the contribution from CP-odd and CP-even states. Moreover doing this analysis with the data from the LHC and fitting an existing physical model with complex mixing phases for CP-even and CP-odd couplings, would give a better understanding and precise measurement of the CP-nature of the Higgs boson coupling and the different values for coefficients in VBF channel and ggF channel would help to distinguish these two production channels in the analysis with the real data from the LHC.

BIBLIOGRAPHY

[1] R. Z. Aben, "*Spinning the Higgs-Spin and parity measurement of the discovered Higgs like boson in the* $H \rightarrow WW \rightarrow lvlv$ *decay mode*", PhD thesis: University of Amsterdam, 2015.

[2] L. Evans and P. Bryant, *LHC Machine*, JINST 3 S08002 (2008).

[3] S. Myers, *The first years of LHC operation*, proceedings of IPAC2012, New Orleans (2012).

[4] R. Vander Geer. "*Search For New Physics Through Single Top*", PhD thesis: University of Amsterdam, 2015.

[5] ATLAS Collaboration, *The ATLAS Experiment at the CERN Large Hadron Collider*, JINST 3 S08003 (2008).

[6] N. Valencic, "Fussing The Vector Boson", PhD thesis:

[7] Antonio Castelli, "*Measuring the Higgs boson mass using event-by-event uncertainties*", PhD thesis: University of Amsterdam, 2015.

[8] ATLAS Collaboration, *ATLAS magnet system TDR. Tech. rep*. Geneva: CERN, 1997.

[9] ATLAS Collaboration, *ATLAS Inner Detector TDR. Tech. rep*. Geneva: CERN, 1997.

[10] ATLAS Collaboration, *ATLAS Liquid Argon Calorimeter TDR. Tech. rep*. Geneva: CERN, 1996.

[11] ATLAS Collaboration, *ATLAS Tile Calorimeter TDR. Tech. rep*. Geneva: CERN, 1996.

[12] ATLAS Collaboration, *ATLAS Muon Spectrometer TDR. Tech. rep*. Geneva: CERN, 1997.

[13] D. Griffiths, "*Introduction to Elementary Particles*", second revised edition, Wiley-VCH (2008).

[14] F. Halzen and A. Martin. "*Quarks and leptons: an introductory course in modern particle physics*." Wiley, 1984.

[15] A. Salam. *Weak and electromagnetic interactions* (1968). Proc. Of the 8th Nobel Symposium on 'elementary particle theory, Relativistic Groups and Analyticity', Stockholm. Sweden, pp. 367-377.

[16] S.L. Glashow. *Partial symmetries of weak interactions*.Nucl.Phys.**22** (1961), pp. 579-588

[17] P.W. Higgs. *Broken Symmetries and the Masses of the Gauge Bosons*, Phys. Rev. Lett. **13**(Oct.1964), pp.508-509.

[18] F. Englert and R. Brout. *Broken Symmetry and the Masses of Gauge Vector Bosons,* Phys.Rev.Lett.13 (Aug.1964), pp.321-323.

[19] P.W. Higgs, *Broken symmetries, massless particles and gauge fields*, Phys. Lett. **12 132**(1964).

[20] J Goldstone, A. Salam and S. Weinberg, *Broken Symmetries*, Phys. Rev**. 127**(1962).

[21] Ivo van Vulpen. *The Standard Model Higgs Boson*. Part of the Lecture Particle Physics II, UvA Particle Physics Master 2013-2014.

[22]

[23] The ATLAS Collaboration, *Observation of a New Particle in the Search for the Standard Model Higgs Boson with the ATLAS Detector at the LHC*, Phys .Lett. **B716** (2012) pp. 1-29, arXiv:1207.7214[hep-ex].

[24] The CMS Collaboration, *Observation of a newboson at a mass of 125 GeV with the CMS experiment at the LHC* (2012), eprint: 1207. 7235.

[25] H.M. Georgi, S. L. Glashow, M.E. Machacek, and D. V. Nanopoulos, *Higgs Bosons from Two Gluon Annihilation in Proton Proton Collision*, Phys, Rev, Lett.**40** (1978) p.692.

[26] R. N. Cahn and S. Dawson, *Production o Very Massive Higgs Bosons,* Phys. Lett. **B136** (1984)P.196, [Erratum: Phys. Lett. B138, 464(1984)].

[27] S. L. Glashow, D.V. Nanopoulos, and A. Yildiz, *Associated Production of Higgs bosons and Z Particles, Phys*. Rev. **D18**(1978)pp. 1724-1727.

[28] Z. Kunszt, *Associated Production of Heavy Higgs Boson with Top Quarks*, Nucl. Phys. **B247**(1984)P. 339.

[29] Higgs plus two jet production via gluon fusion as a signal at the CERN LHC G. Kl¨amke and D. Zeppenfeld. arXiv:0703202v1[hep-ph].

[30] J. R. Andersen, K. Arnold, D. Zeppenfeld, *Azimuthal Angle Correlations for Higgs Boson plus Multi-Jet Events* (2010)arxiv:1001.3822.

[31] LHC Higgs Cross Section Working Group. TWiki, CERN.

[32] S. Gadatsch, "*The Higgs Boson"*, PhD thesis: University of Amsterdam, 2015.

[33] M. Kobayashi, T. Maskawa; Maskawa (1973).*CP-Violation in the Renormalizable Theory of Weak Interaction*. Progress of Theoretical Physics.

[34] F. Demartin, F. Maltoni, K. Mawatari, B. Page, and M. Zaro*, Higgs characterisation at NLO in QCD: CP properties of the top-quark Yukawa interaction.(2014).* arXiv:1407.5089v2[hep-ph].

[35] Artoisenet P, de Aquino P, Demartin F, Frederix R, Frixione S, et al. *A framework for Higgs characterisation*. JHEP. 2013; 1311: 043. doi: 10.1007/JHEP11(2013)043.

[36] V. Hankele, G. Kl¨amke, D. Zeppenfeld. *Anomalous Higgs boson couplings in vector boson fusion at the CERN LHC.* arXiv:0609075v2[hep-ph].

[37] V. Hankele, G. Kl¨amke, and D. Zeppenfeld. *Higgs+2 Jets As A Probe For CP Properties*. arXiv:hep-ph/0605117v1 10 May 2006KA–TP–05–2006.

[38] A. Djouadi, R.M. Godbole, B. Mellado and K. Mohan. *Probing the spin-parity of the Higgs boson via jet kinematics in vector boson fusion*. arXiv:hep-ph/1301.4965v2. Physics Letters **B 723** (2013), pp. 307-313.